DIMENSIONLESS PRESSURE AND PRESSURE DRIVATIVE RESPONSES OF A VERTICAL WELL COMPLETED IN A RESERVIOR WITH IMPERMEABLE BOUNCARY INCLINED AT RIGHT ANGLE

BY

BLESSING OJONE YAKUBU

ENG 1805597

DEPARTMENT OF PETROLEUM ENGINEERING

FACULTY OF ENGINEERING

UNIVERSITY OF BENIN

BENIN CITY

APRIL, 2024

DIMENSIONLESS PRESSURE AND PRESSURE DRIVATIVE RESPONSES OF A VERTICAL WELL COMPLETED IN A RESERVIOR WITH IMPERMEABLE BOUNCARY INCLINED AT RIGHT ANGLE

BY

BLESSING OJONE YAKUBU

ENG 1805597

A PROJECT REPORT SUBMITTED TO THE DEPARTMENT OF PETROLEUM ENGINEERING

IN PARTIAL FULFILLMENT OF THE REQUIREMENTS FOR THE AWARD OF BACHELOR OF ENGINEERING (B.ENG) DEGREE IN PETROLEUM ENGINEERING

DEPARTMENT OF PETROLEUM ENGINEERING

FACULTY OF ENGINEERING

UNIVERSITY OF BENIN

BENIN CITY

APRIL, 2024

CERTIFICATION

This is to certify that this thesis titled "" was carried out by BLESSING OJONE YAKUBU with matriculation number ENG 1805597 of the Department of Petroleum Engineering, Faculty of Engineering, University of Benin in partial fulfilment of the requirements for the Award of the Degree, Bachelor of Engineering (B.ENG) under the guidance of Professor (Engr.) K. O. Bello.

_____	_____
PROF. (ENGR.) E. S. ADEWOLE	**DATE**
(PROJECT SUPERVISOR)	
_____	_____
DR. (ENGR.) O. A. TAIWO	**DATE**
(PROJECT COORDINATOR)	
_____	_____
DR. (ENGR.) I. OHENHEN	**DATE**
(HEAD OF DEPARTMENT)	
_____	_____
PROF. S. O. ISEHUNWA	**DATE**
(EXTERNAL SUPERVISOR)	

DEDICATION

This work is dedicated God almighty, the source who has made my life beautiful. I dedicate this work to my parents, whose unwavering support, love, and encouragement have been the cornerstone to my academic achievements. Their sacrifices and belief in my abilities have shaped me into the person I am today.

ACKNOWLEDGEMENT

Firstly, I owe a debt of gratitude to the Almighty God for His manifold grace and mercy to me and for seeing me through from the very beginning up to this present stage of my life and career. I thank my parents Mr. and Mrs. Glory Yakubu and my entire family(King David,Favour,Dorcas and Deborah), Mr David Ameh and family,my aunty Augustina Edeh-Ugedeojo and family,James Alleh immensely for their support, love, care, advice, guidance and all before, during and after this period. I appreciate it all.

Special thanks to Prof. E. S. Adewole, my supervisor, for always supporting me, mentoring me, giving me recommendations, and assisting me throughout this journey. His encouragement and efforts were crucial in helping me progress. I truly appreciate everything Additionally, I extend my gratitude to my friends and classmates for their camaraderie and shared experiences that enriched my learning journey

Lastly, I want to thank the management and staff of the Department of Petroleum Engineering at the University of Benin, particularly Associate Professor Sunny Agbons Igbinere, Dr. Ikponmwosa Ohenhen, Dr. Blessing Otamere, Mr. Benedict Ikponmwosa Usiosefe, Mr. Osagie Ehiosu, Mr. Isuk, and many others, also Engr. Martins. They provided me with opportunities and played a significant role in preparing me to achieve this milestone.

TABLE OF CONTENT

LIST OF TABLES

LIST OF FIGURES

ABSTRACT

Dimensionless pressure and its derivatives contribute immensely to understanding the reservoir boundaries, efficient well design, production scheduling, and completion for optimum recovery from the reservoir. It is imperative to sufficiently anticipate the presence of a reservoir border and its approach pattern towards the wellbore since such a boundary poses a constant pressure threat to the production of oil or gas. Dimensionless pressures and their derivatives for a vertical well finished inside two inclined sealing border supports are presented in this study. The inclination angle is 90 degrees or the right angle. As a result, by superimposing the dimensionless pressures of every image well onto a single object well, a generalized dimensionless pressure and derivatives expressions are obtained. Therefore, the principal inputs into the dimensionless pressures and dimensionless pressure derivatives obtained are the distances of each well from the object well and the sign of each image, taken through a counterclockwise path from the object well. Both the object's wellbore skin and its storage are taken into account. Plotting the solutions results in type curves. The results demonstrate how the angle of inclination of the sealing boundary affects dimensionless derivatives and dimensionless pressure. At late dimensionless times, the dimensionless pressures show a distinct gradient. Late dimensionless times result in a collapse of the derivatives to zero. The proximity of the well to the boundaries and the angle of inclination are critical factors determining the rate of this collapse. Notably, wells situated further from the sealing boundary exhibit prolonged periods of stable production compared to those closer to the boundary. These insights have direct implications for designing wells and managing reservoirs with inclined boundaries, potentially enhancing production longevity and efficiency.

CHAPTER ONE

1 INTRODUCTION

1.1 BACKGROUND OF STUDY

The extraction of hydrocarbons from subsurface reservoirs is a linchpin of the global energy landscape, fueling the ever-increasing demand for energy. These reservoirs, geological formations capable of storing oil and gas, are typically situated deep beneath the Earth's crust. These geological formations, often located several kilometers beneath the Earth's surface, are repositories of the world's hydrocarbon wealth. The process of drilling wells to access these reservoirs is a sophisticated engineering challenge, with the efficiency of hydrocarbon recovery hinging on numerous factors such as flow dynamics, pressure management, and production optimization The success of these wells is measured by various factors, including flow rates, pressure stability, and overall production efficacy. Therefore, a deep comprehension of reservoir dynamics and well behavior is paramount to maximizing the extraction of resources and optimizing production methodologies. These geological formations, often located several kilometers beneath the Earth's surface, are repositories of the world's hydrocarbon wealth. The process of drilling wells to access these reservoirs is a sophisticated engineering challenge, with the efficiency of hydrocarbon recovery hinging on numerous factors such as flow dynamics, pressure management, and production optimization.

The role of petroleum engineering in this endeavor is paramount, as it encompasses the study and application of principles that enable the effective extraction of oil and gas. One of the critical aspects of this field is understanding the behavior of fluid pressure within reservoirs, which is a direct indicator of the well's performance and the reservoir's potential. The presence of impermeable boundaries, particularly those inclined at right angles, introduces a complex set of variables that must be navigated to optimize production.

These impermeable boundaries, often natural geological features such as faults or artificially created barriers, can significantly influence the flow of hydrocarbons within the reservoir. The inclination of these boundaries at right angles to the wellbore presents unique challenges in predicting pressure behavior and, consequently, in designing wells that can maximize recovery while minimizing risks.

Dimensionless pressure analysis emerges as a crucial tool in this context. By employing dimensionless pressure and pressure derivative responses, engineers can normalize the data, removing the influence of scale and allowing for a more accurate comparison across different well and reservoir conditions.(Olaya-Marin et al., 2020) This form of analysis is particularly useful in reservoirs with impermeable boundaries, as it provides insights into how these barriers affect fluid flow and pressure distribution.

The study of dimensionless pressure and its derivatives in vertical wells completed within reservoirs with inclined impermeable boundaries is not merely an academic exercise; it

has profound practical implications. The ability to predict how the pressure will behave in response to such boundaries can lead to more informed decisions regarding well placement, drilling direction, and completion strategies. It can also help identify potential issues such as early water breakthrough or gas coning, which can adversely affect production.

Furthermore, the analysis of dimensionless pressure responses aids in the assessment of reservoir connectivity and compartmentalization. This is essential for developing effective reservoir management strategies, as it allows for the identification of discrete hydrocarbon-bearing zones and the optimization of production from each zone.

Incorporating the principles of dimensionless pressure analysis into well design and reservoir management is a testament to the evolution of petroleum engineering as a discipline. It reflects the industry's move towards more sophisticated, data-driven approaches that can navigate the complexities of subsurface environments.(Khan et al., 2020) As the energy demand continues to grow, and as the challenges of extraction become more intricate, the insights provided by dimensionless pressure analysis will become increasingly valuable.

This research contributes to the body of knowledge in petroleum engineering by providing a comprehensive analysis of dimensionless pressure and pressure derivative responses in a specific and challenging reservoir context. The findings of this study have the potential to influence well design and production strategies, leading to more efficient and sustainable hydrocarbon recovery practices.

1.2 PROBLEM STAEMENT

Previous studies have focused on vertical wells with inclined constant-pressure boundaries or inclined sealing faults, but none have investigated wells in reservoirs with impermeable boundaries

1.3 AIM AND OBJECTIVE

The proposed objectives are;

- To develop analytical solutions for dimensionless pressure and pressure derivatives for a vertical well in a reservoir bounded within an impermeable boundary.
- To investigate the effects of boundary inclination, well location, wellbore skin, and reservoir properties on the dimensionless pressure and pressure derivative behavior of the vertical well.
- To compare the analytical solutions with existing numerical and experimental data and validate their accuracy and applicability.
- To provide useful guidelines and recommendations for reservoir characterization, well testing, and production optimization of vertical wells in reservoirs with impermeable boundaries.
- To investigate effect of well location on well performance.
- To determine the flow period in a vertical well inclined at right angle

1.4 SCOPE OF STUDY

The proposed methodology is to use the superposition principle to analyze the observation wells and their mirror images, and apply statistical methods to evaluate the quality of the results under different conditions. Python will be used as the programming language for this analysis.

The achievement of these objectives will help enhance understanding of the complex flow behavior of vertical wells in reservoirs with impermeable boundaries, which are common in unconventional oil and gas resources, and provide a reliable and efficient tool for predicting and evaluating the performance of vertical wells in such reservoirs, which can help optimize well design, placement, and operation

CHAPTER TWO

2 LITERATURE REVIEW

2.1 RESERVIOR BOUNDARY

Reservoir boundary conditions are a critical aspect of reservoir simulation and management, as they define the limits and behavior of fluid flow within the reservoir. The reservoir's overall performance, fluid flow, and pressure distribution can all be greatly impacted by these circumstances.

In the context of reservoir engineering, boundary conditions are typically categorized into two types:

1. **Closed Boundary Conditions**: These imply that there is no flow across the boundary. The reservoir is considered isolated, and the fluid within cannot move beyond its limits. This condition is often used in simulations to represent a sealed reservoir with no external influence. (Lu et al., 2023)
2. **Constant Pressure Boundary Conditions**: These suggest that the pressure at the boundary remains constant over time. This could represent a reservoir in contact with a much larger system, such as an aquifer or another reservoir, where the pressure is maintained by the vast volume of the external system.(Lu et al., 2023)

Another study examines how reservoir border conditions, drainage form, and well site influence vertical well productivity. It indicates that drainage area and boundary conditions have a major impact on well production, and that productivity varies only somewhat with drainage shape and well location.

2.2 FLOW TYPE

The “flow period” in reservoir engineering refers to the duration of time during which fluid is actively moving within the reservoir. This term can be associated with different flow regimes that describe how the pressure and fluid distribution change over time. Here’s a brief explanation of the main flow regimes:

- **Steady-State Flow**: The flow regime is classified as a steady-state flow if the pressure at every site in the reservoir remains constant, that is, does not change over time. Mathematically, this condition is expressed as;

  $$\left(\frac{\partial \mathrm{p}}{\partial \mathrm{t}}\right)\mathrm{i} = 0$$

  According to the equation above, the rate of change of pressure p with respect to time t at any given location I is zero. In reservoirs, steady-state flow occurs only

when the reservoir is fully recharged and supported by robust aquifer or pressure maintenance activities. Factors that affect steady state include pressure, velocity

- **Unsteady-State Flow**: Also known as transient flow or infinite acting, this regime is characterized by changing pressures throughout the reservoir over time at any position in the reservoir is not zero or constant. It is typical in the early phases of production while the reservoir is becoming used to the new fluid withdrawal conditions. Mathematically, this condition is expressed as;

$$\left(\frac{\partial p}{\partial t}\right) i = f(i, t)$$

In this period, there is majorly clean production. It is he most preferred flow period(Matthews, 1986). Factors that affect steady state include compressibility, skin, wellbore storage.

- **Pseudosteady-State Flow**: This regime is observed when a reservoir is bounded by constant pressure boundaries, such as an aquifer. In this instance, the pressure distribution approaches a quasi-steady state while the average reservoir pressure decreases Mathematically, this condition is expressed as;

$$\left(\frac{\partial p}{\partial t}\right) i = \text{constant}$$

Factors that affect steady state include compressibility, drainage boundary, production rate.

The flow period is crucial for understanding and predicting reservoir performance, as it impacts the pressure distribution, recovery factor, and overall production strategy. Accurate modeling of the flow period helps in making informed decisions for optimal reservoir management(H. et al., n.d.)

2.3 SUPERPOSITION PRINCIPLE

The principle states that the total pressure drop in a well is the sum of the pressure drop due to rate changes experienced by the well. The rate change could be due to production(+ve), injection(-ve) or shut in (zero). **S**uperposition is used to analyze the pressure behavior in a reservoir due to multiple wells, changing production rates, or varying boundary conditions. (Ganat, 2023)

2.3.1 Application of Superposition:

1. **Multiple Wells:** When multiple wells are producing simultaneously, the pressure response at any point in the reservoir is the sum of the pressure changes caused by each well.
2. **Variable Rates:** Superposition can be used to calculate the pressure distribution in a reservoir when production rates vary over time. The pressure response to a variable rate can be constructed by superposing the responses to a series of constant-rate flows.
3. **Boundary Changes:** The principle also applies when reservoir boundaries change, such as when new faults are activated or existing ones are sealed.

2.3.2 Mathematical Formulation:

The mathematical formulation of superposition in reservoir engineering involves the use of the diffusivity equation, which describes fluid flow in porous media. The equation can be linearized under certain conditions, allowing the use of superposition

- Superposition in single well

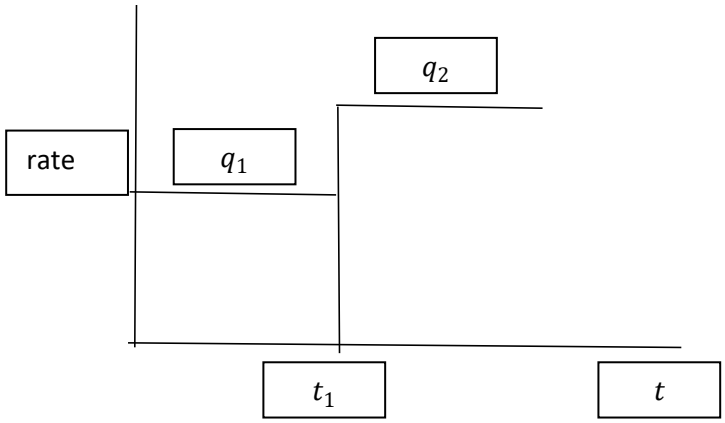

Figure 2.1 Rate against time

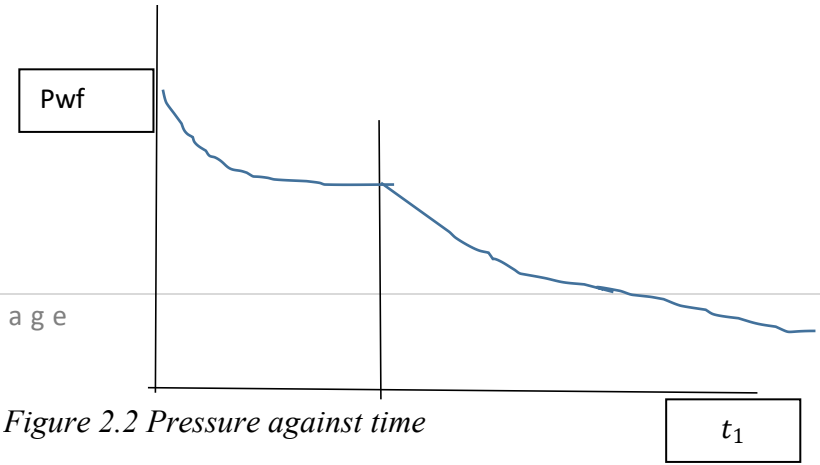

Figure 2.2 Pressure against time

$$\Delta P_T = -\frac{70.6 q_1 \mu B}{kh}\left[Ei\left(-\frac{948 \emptyset \mu c_t {r_w}^2}{kt}\right) - 2s\right]$$
$$-\frac{70.6(q_2 - q_1)\mu B}{kh}\left[Ei\left(-\frac{948 \emptyset \mu c_t {r_w}^2}{k(t - t_1)}\right) - 2s\right]$$

- Superposition in multiple well

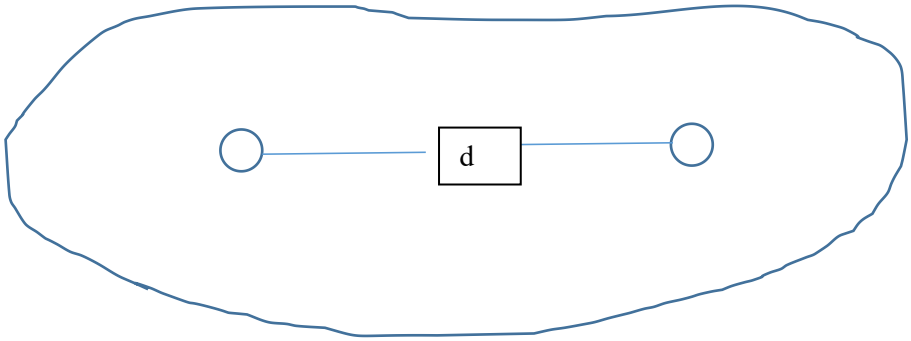

Figure 2.3 Image of the wells location

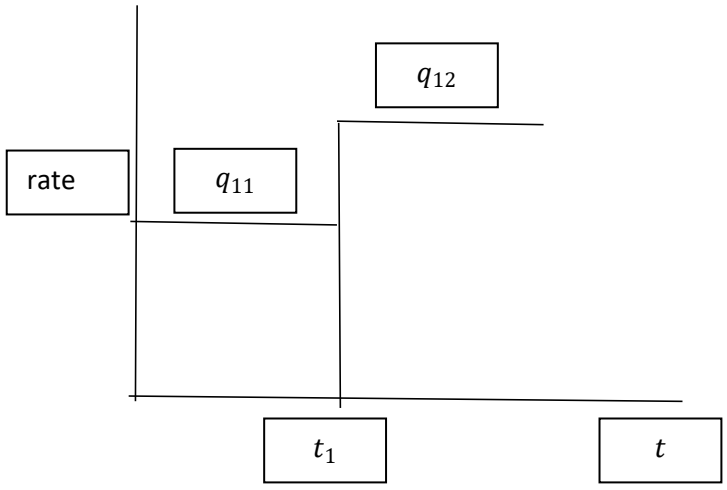

Figure 2.4 Rate against time

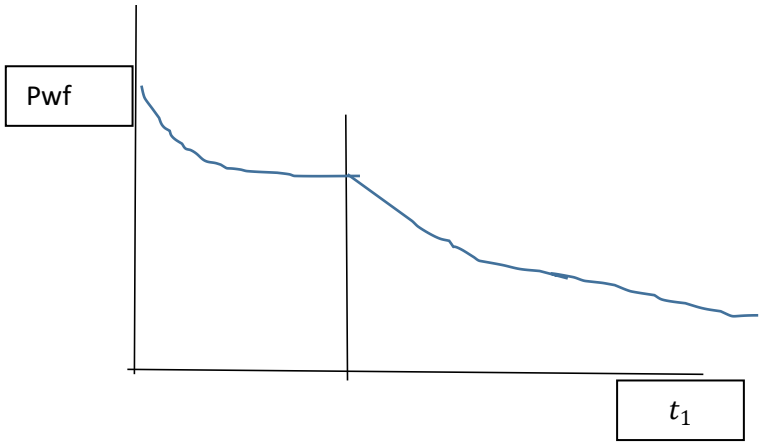

Figure 2.5 Pressure against time

$$\Delta P_{T,1} = \Delta P_{1,1} + \Delta P_{1,2}$$

$$\Delta P_{1,1} = -\frac{70.6 q_{11} \mu B}{kh}\left[Ei\left(-\frac{948 \emptyset \mu c_t {r_{w1}}^2}{kt}\right) - 2s_1\right] - \frac{70.6(q_{12} - q_{11})\mu B}{kh}\left[Ei\left(-\frac{948 \emptyset \mu c_t {r_w}^2}{k(t - t_1)}\right) - 2s_1\right]$$

$$\Delta P_{1,2} = -\frac{70.6 q_{21} \mu B}{kh}\left[Ei\left(-\frac{948 \emptyset \mu c_t d^2}{kt}\right)\right] - \frac{70.6(q_2 - q_1)\mu B}{kh}\left[Ei\left(-\frac{948 \emptyset \mu c_t d^2}{k(t - t_1)}\right)\right]$$

2.3.3 Application of Superposition:

- To estimate reservoir remaining pressure
- To design pressure buildup test analysis procedure
- To design interference test analysis procedure
- To investigate reservoir external boundary type
- To estimate the angle of inclination of reservoir boundaries
- To count the number of interfering wells in a reservoir or reservoirs in communication
- To estimate the distance between interfering wells

2.3.4 Limitations:

- **Linearity:** The principle of superposition is only valid for linear systems. Non-linear effects, such as those caused by significant pressure changes, may require more complex analysis.
- **Homogeneity:** It assumes the reservoir is homogeneous. Heterogeneities can lead to deviations from the predicted behavior.

2.4 PRESSURE DROP

Pressure drop is the reduction in pressure that happens within an underground reservoir when fluids (such as oil, gas, or water) are generated or injected. Understanding pressure drop in reservoirs is critical for forecasting reservoir behavior, improving production techniques, calculating reserves, and assuring the economic sustainability of hydrocarbon recovery projects(Jr et al., n.d.).

2.4.1 Causes of Pressure Drop in Reservoirs

1. **Production Rate**: As hydrocarbons are produced from a reservoir, the pressure within the reservoir lowers due to reduced fluid volume and energy depletion.

2. **Fluid Expansion**: When reservoir fluids (oil, gas, and water) travel from high-pressure to low-pressure zones, they expand, causing pressure to decrease. This expansion can take place within the reservoir rock matrix or in the wellbore and surface facilities.

3. **Reservoir Depletion:** As the initially trapped fluids are evacuated, reservoir pressure gradually decreases. The depletion is influenced by reservoir shape, fluid characteristics, and production rates.

4. **Fluid Movement**: Fluid movement inside the reservoir, including fluid displacement caused by injected fluids (e.g., water injection for pressure maintenance or better oil recovery) can cause pressure variations and drop in certain areas.

2.5 DIMENSIONLESS PRESSURE AND ITS DERIVATIVE

2.5.1 DIMENSIONLESS PRESSURE

Dimensionless pressure is a normalized measure used to assess well performance and pressure behavior in reservoirs. It enables us to compare pressure data from various wells, reservoirs, and conditions without being influenced by particular units. The dimensionless pressure is usually represented as pD. Dimensionless pressure and its derivatives can provide a full understanding of reservoir pressure distribution and variation across time, allowing for improved well performance and recovery. (Abbaszadeh et al., n.d.). Dimensionless pressures offer a unique interpretation of pressure data by removing the impacts of wellbore storage and skin. They can be defined as the ratio of actual pressure to characteristic pressure.

$$\text{Dimensionless pressure} = p_D = \frac{kh\Delta p}{141.2q\mu B} = \frac{kh(p_i - p_{wf})}{141.2q\mu B} = \frac{kh(p_i - p_{r,t})}{141.2q\mu B}$$

2.5.1.1 Importance of Dimensionless pressure and its derivatives

- Dimensionless pressure helps us understand the transient behavior of reservoirs during production or injection.
- It aids in identifying wellbore effects (such as skin) and reservoir properties (such as permeability).
- By analyzing dimensionless pressure curves, engineers can assess well performance, estimate reservoir parameters, and optimize production strategies

2.5.1.2 Mathematical expression of dimensionless pressure

The dimensionless pressure expression for the object well is:

Total dimensionless pressure drop in the object = dimensionless pressure drop in the object well well due to flow in the object well+dimensionless pressure drop in the object well due to flow in image well 1+dimensionless pressure drop in the object well due to flow in image well 2+…. (Eziuzor et al., n.d.)

Mathematically, for a vertical well,

$$p_{Dow} = p_{Dow,\,ow} + p_{Dow,\,iw1} + p_{Dow,\,iw2} + \cdots\cdots\cdots$$

$$p_{Dow} = -\frac{1}{2}\left[Ei\left(-\frac{1}{4t_D/cD}\right) - s_{ow} + Ei\left(-\frac{d_1^2}{4t_D}\right) + Ei\left(-\frac{d_2^2}{4t_D}\right) + Ei\left(-\frac{d_3^2}{4t_D}\right)\cdots\cdots\cdots\right]$$

Mathematically, for horizontal well

$$p_{Dow} = p_{Dow,\,ow} + p_{Dow,\,iw1} + p_{Dow,\,iw2} + \cdots\cdots\cdots$$

$$p_{Dow} = -\frac{\propto}{4L_D}\left[Ei\left(-\frac{r_{wD}^2}{4t_D}\right) + s_{ow} + Ei\left(-\frac{d_1^2}{4t_D}\right) + Ei\left(-\frac{d_2^2}{4t_D}\right) + Ei\left(-\frac{d_3^2}{4t_D}\right)\cdots\cdots\cdots\right]$$

2.5.1.3 Applications of Dimensionless Pressure:

- Well Testing: During well testing, dimensionless pressure is a key parameter.
- Pressure-Transient Analysis: Dimensionless pressure curves interpret pressure buildup and drawdown tests.
- Reservoir Characterization: Comparing dimensionless pressure across wells assists in reservoir modeling.

2.5.2 DIMENSIONLESS PRESSURE DERIVATES

- These plots display dimensionless pressure ((pD)) and its derivative ((pD')) on log-log axes.

- They serve as diagnostic tools in reservoir engineering.
- By analyzing these plots, we can:
    - Identify different flow periods within a well.
    - Clearly delineate the wellbore storage period.
    - Determine the type of reservoir external boundary

$$\text{Dimnesionless pressure derivative} = p_D' = t_D \frac{\partial p_D}{\partial t_D} = \frac{\partial p_D}{\ln \partial t_D}$$

2.6 OTHER WORKS DONE

Over the years a lot of work has been done relating to dimensionless pressure and its derivatives for both vertical and horizontal well.

1. Ojukwu et al. (2023) conducted a study titled "Dimensionless Pressures and their Derivatives for a Vertical Well Completed within a Pair of Inclined Constant-Pressure Boundaries," which aimed to understand reservoir boundary effects, efficient well design, completion, and production scheduling for optimal recovery. Their investigation specifically focused on a vertical well completed within a pair of inclined constant-pressure boundaries (CPBs). The methodology involved varying the angle of inclination of the CPBs from 0 to 360 degrees and deriving generalized expressions for dimensionless pressure and derivatives by superimposing pressures from image wells onto an object well. Notably, only the object wellbore skin was considered in the analysis, excluding storage effects. The results revealed that both dimensionless pressure and dimensionless derivatives are sensitive to the angle of inclination of the CPBs. Additionally, dimensionless pressures exhibited a unique gradient at late dimensionless times, while the derivatives eventually collapsed to zero during late dimensionless times. The rate of this collapse depended on factors such as the distance between the object well and the boundaries and the boundary inclination angle. Moreover, the study observed that wells completed farther away from the CPBs experienced longer periods of unperturbed production compared to those nearer the boundaries..(Ojukwu et al., 2023)

2. In another paper titled "Pressure and Pressure Derivative Interpretation for Vertical Wells in Naturally Fractured and Compressible Formations," Escobar et al. (2020) focused on interpreting well tests in reservoirs with natural fractures and compressibility, aiming to determine crucial parameters such as permeability, permeability modulus, and geomechanical skin factor. They introduced novel expressions that utilize the slope of pressure derivatives during the radial flow regime to calculate these reservoir parameters, alongside corrections for the minimum point and the intercept during the transition period and radial flow regime. This methodology was successfully applied to synthetic examples, emphasizing its potential to enhance the understanding of stress effects on

permeability and improve parameter determination in naturally fractured reservoirs.. (Escobar et al., 2020)

3. The study by Ogbamikhumi et al. (2021) investigates dimensionless pressure gradients and dimensionless pressure derivatives for horizontal and vertical wells completed within a pair of no-flow boundaries inclined at a general angle 'θ'. The methodology utilizes the infinite-acting flow solution for each well, considers image distances due to inclinations, and applies the superposition principle to calculate the total pressure drop from both object and image wells. Key observations include dimensionless pressure gradients for horizontal wells being approximately after very early time, with representing the number of images formed due to inclination. Additionally, dimensionless pressure derivatives are observed for both central and off-centered horizontal well locations. It is noted that central well locations do not significantly affect horizontal well productivity across all inclinations. Moreover, the magnitudes of dimensionless pressure drop and dimensionless pressure derivatives are maximum at the farthest image distances, and these characteristics remain unaffected by well stand-off for horizontal wells.. (Ogbamikhumi et al., n.d.)

4. Edobhiye and Adewole (2014) investigated the effects of both wellbore and reservoir properties on dimensionless pressure and dimensionless pressure derivatives, focusing on a horizontal well within a reservoir subjected to bottom water, gas cap, and single edge water drive mechanisms. They found that dimensionless pressure increases with reservoir thickness. Additionally, they observed that dimensionless well stand-off does not significantly affect dimensionless pressure and its derivative. Furthermore, they noted an inverse relationship between dimensionless wellbore radius and dimensionless well length. The study also highlighted that infinite conductivity and uniform flux completions have no impact on dimensionless pressure. Overall, these insights provide valuable guidance for correct well design, completion, and perforation locations to prolong clean oil production.(Edobhiye & Adewole, 2014)

5. Kuchuk et al. (1991) conducted a study titled "Pressure Transient Behavior of Horizontal Wells in Bounded Reservoirs with Gas Cap and Aquifer," which provides valuable insights into the pressure behavior of horizontal wells in reservoirs with specific characteristics. The objective of the study is to monitor the performance of horizontal wells and characterize the reservoirs surrounding them, particularly focusing on reservoirs bounded by vertical constant pressure boundaries and completely bounded reservoirs in all X-, Y-, and Z-directions coupled with vertical constant pressure boundaries. The authors present an analytical solution for the pressure transient response of horizontal wells, assuming the reservoir is anisotropic, rectangular, and homogeneous, and includes boundaries such as a gas cap, an aquifer, and lateral no-flow boundaries. The methodology employs Green's and source function methods, combined with Newman's product method, and utilizes type curves analysis to understand different flow regimes exhibited during the transient behavior. Observations from

the study highlight that pressure behavior and flow regimes are influenced by the type of outer boundaries, the distance of the well to the nearest boundary, and the length of the horizontal well itself. The study also notes that common flow regimes associated with horizontal wells may be masked by constant pressure behavior. The practical implications underscore the advantages of horizontal wells, including increased productivity, reduced effects of damaged zones, and higher oil recovery due to better sweep efficiency, and emphasize the importance of analytical models based on transient pressure analysis for assessing horizontal well productivity and reservoir characterization.(Kuchuk et al., 1991)

2.7 RESEARCH GAP

The research bridges a significant knowledge gap regarding dimensionless pressure and pressure derivative responses for vertical wells in reservoirs with inclined and impermeable boundaries, specifically angled at 90 degrees. It highlights key aspects to improve our understanding of pressure transient behavior within such reservoirs. Firstly, it emphasizes the influence of wellbore storage on pressure responses during transients, stressing the need for accurate assessments. Secondly, it underscores the importance of considering skin effects, often overlooked, which can distort permeability near the well. Thirdly, it delves into the unique flow patterns of vertical wells in these reservoirs, which is crucial for optimizing reservoir sweep efficiency. Additionally, it recognizes strategic well placement relative to reservoir boundaries as a key factor shaping transient behavior and drainage patterns. By addressing these aspects, the research significantly advances our understanding of transient behavior in bounded reservoirs, aiming to enhance reservoir management practices and optimize oil and gas production efficiency through improved modeling and tailored production strategies for vertical wells.

Sent by you: The research bridges a significant knowledge gap regarding dimensionless pressure and pressure derivative responses for vertical wells in reservoirs with inclined and impermeable boundaries, specifically angled at 90 degrees. It highlights key aspects to improve our understanding of pressure transient behavior within such reservoirs. Firstly, it emphasizes the influence of wellbore storage on pressure responses during transients, stressing the need for accurate assessments. Secondly, it underscores the importance of considering skin effects, often overlooked, which can distort permeability near the well. Thirdly, it delves into the unique flow patterns of vertical wells in these reservoirs, which is crucial for optimizing reservoir sweep efficiency. Additionally, it recognizes strategic well placement relative to reservoir boundaries as a key factor shaping transient behavior and drainage patterns. By addressing these aspects, the research significantly advances our understanding of transient behavior in bounded reservoirs, aiming to enhance reservoir management practices and optimize oil and gas production efficiency through improved modeling and tailored production strategies for vertical wells.

CHAPTER THREE

3 METHODOLOGY

Given an infinite acting flow, the expression for dimensionless pressure drop in the wellbore is given in dimensionless form:

$$P_{DOW} = -\frac{1}{2}\mathrm{Ei}\left[\frac{r_D^2}{4t_D}\right] + s \quad (3.1)$$

While the dimensionless pressure derivative is given as:

$$P'_{DOW} = -\frac{1}{2}\exp\left[-\frac{r_D^2}{4t_D}\right] \quad (3.2)$$

Equation (3.1) above represents the dimensionless pressure decline in the wellbore, taking into account only the wellbore skin rather than wellbore storage.

Wells communicate with one another and are impacted by their surroundings; therefore, well positioning must be strategic to secure long-term oil production. We would need to investigate the boundary conditions, which in this case are a pair of inclined sealed faults. A vertical well between two sealing faults produces images that correlate to the degree of inclination; the larger the angle of inclination, the fewer the images created; images are formed until they converge at a point, producing polygons.(Kartoatmodjo, 2016)

A proposed model relating the number of images to the angle of inclination is:

$$n = \frac{360}{\theta} - 1$$

where n is the number of images and

θ is the angle of inclination.

Well, images must be considered to be a pressure drop across wells becomes the addition of the pressure drop of the object well and the image wells.

Calculation of slope is given the formula

$$1.1513(1 + n) = m$$

where m is slope and n is the number of image wells

When a vertical well is completed between two sealing boundaries inclined at an angle θ, image wells are created perpendicular to the object well through the impermeable boundary in a circular direction. The next picture well is formed at a perpendicular distance from the preceding one. The number of image wells formed depends on the angle of inclination.

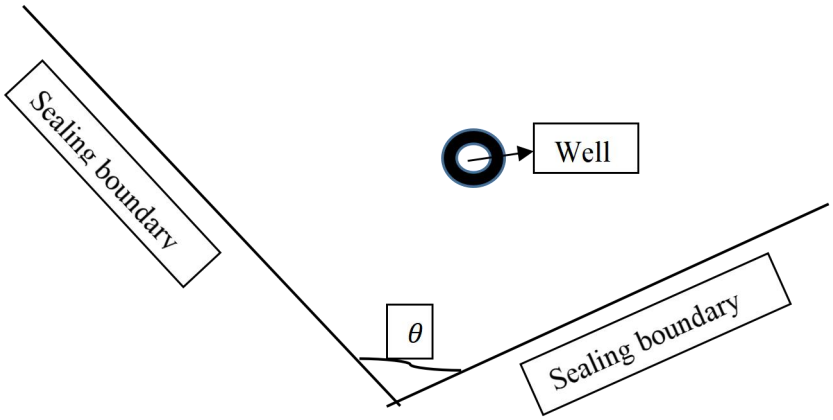

Figure 3.1 Schematic of a vertical well completed within a sealing boundary

The pressure drop in the object well is affected by the pressure drop in the image wells. Therefore, using the superposition principle, the pressure drop in the object well equals the sum of the pressure drops in the object and image wells. In dimensionless pressure form, the total pressure decrease within a pair of faults inclined at an angle can be expressed as:

$$P_{DOW} = P_{DOW1} + P_{DOW2} + P_{DOW3} + P_{DOW4}$$
(3)

Dimensionless pressure across a well inclined at an angleθ is given as:

$$P_{DOW} = -\frac{1}{2}\mathrm{Ei}\left[\frac{r_D^2}{\frac{4t_D}{C_D}}\right] - \frac{1}{2}\mathrm{Ei}\left[\frac{d^1}{\frac{4t_D}{C_D}}\right] - \frac{1}{2}\mathrm{Ei}\left[\frac{d^2}{\frac{4t_D}{C_D}}\right] + \ldots$$
(3.4)

While the dimensionless pressure derivative is given as

$$P'_{DOW} = -\frac{1}{2}\exp\left[-\frac{r_D^2}{4t_D}\right] - \frac{1}{2}\mathrm{Ei}\left[\frac{d^1}{\frac{4t_D}{C_D}}\right] - \frac{1}{2}\mathrm{Ei}\left[\frac{d^2}{\frac{4t_D}{C_D}}\right] + \ldots$$
(3.5)

Consider a vertical well completed between a pair of constant pressure boundaries inclined at the right angle. A total of three image wells were produced (n=3). Figure 1 below shows a vertical well completed within an impermeable boundary inclined at right angle.

3.1 HOW TO LOCATE THE IMAGE WELL

- Reproduce the mirror combination to form a polygon, it depends on the angle of inclination.
- Drop a line from the object well to the first mirror moving in a clockwise direction.

- The first image distance is equal to the object distance from the first mirror principle of plain mirror.
- Repeat the procedure above until the last image become an object of bottom mirror

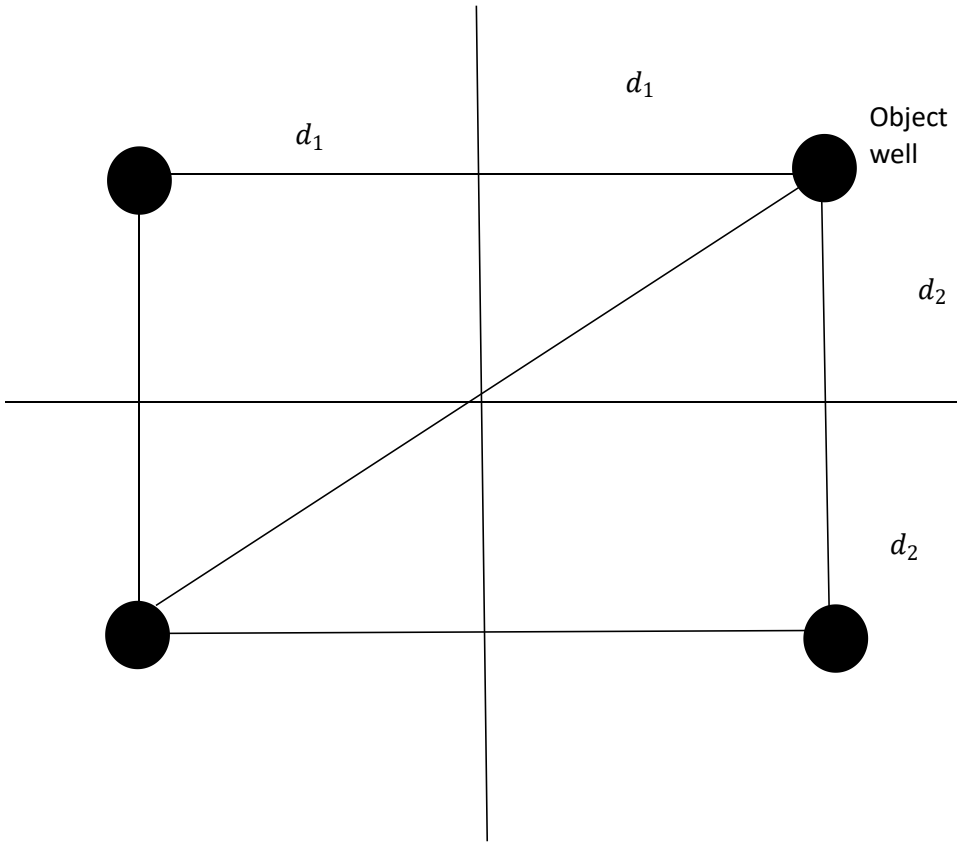

Figure 3.2 Diagram of the observation well

- Measure the direct image distance from the object well.

where

$$I_1 = 2d_1$$

$$I_3 = 2d_3$$

$$I_3 = \sqrt{2{d_1}^2 + 2{d_3}^2} = 2d_2$$

Where I_1 and I_2 are I_3 are the image wells

3.2 Dimensionless pressure across a well inclined at right angle

Dimensionless pressure across a well inclined at right angle is given as:

$$P_{DOW} = -\frac{1}{2}\text{Ei}\left[\frac{r_D^2}{\frac{4t_D}{C_D}}\right] + s - \frac{1}{2}\text{Ei}\left[\frac{{d_1}^2}{4t_D}\right] - \frac{1}{2}\text{Ei}\left[\frac{{d_2}^2}{4t_D}\right] - \frac{1}{2}\text{Ei}\left[\frac{{d_3}^2}{4t_D}\right]$$

$$P_{DOW} = -\frac{1}{2}\left[\text{Ei}\left[\frac{r_D^2}{\frac{4t_D}{C_D}}\right] + \text{Ei}\left[\frac{{d_1}^2}{4t_D}\right] + \text{Ei}\left[\frac{{d_2}^2}{4t_D}\right] + \text{Ei}\left[\frac{{d_3}^2}{4t_D}\right] + 2s\right]$$

(3.6)

While the dimensionless pressure derivative is given as

$$P'_{DOW} = -\frac{1}{2}\exp\left[-\frac{r_D^2}{4t_D}\right] - \frac{1}{2}\exp\left[\frac{{d_1}^2}{4t_D}\right] - \frac{1}{2}\exp\left[\frac{{d_2}^2}{4t_D}\right] - \frac{1}{2}\exp\left[\frac{{d_3}^2}{4t_D}\right]$$

$$P'_{DOW} = -\frac{1}{2}\left[\exp\left[-\frac{r_D^2}{4t_D}\right] + \exp\left[\frac{{d_1}^2}{4t_D}\right] + \exp\left[\frac{{d_2}^2}{4t_D}\right] + \exp\left[\frac{{d_3}^2}{4t_D}\right]\right]$$

(3.7)

When calculating for Ei , the Ei table for values greater than 0.01, and for $i(x) = \ln 1.781x$, when $x \leq 0.01$, and use Gauss Lagurre to find values not on the Ei table(E.S & O., n.d.)

3.3 General computing procedure

- Select angle of inclination, object well distance from the boundary
- Compute P_{DOW}
- Compute $\frac{dP_{DOW}}{dt_D}$
- Compute across different period on the curve.
- Locate the image well
- Measure the image well.
- Vary object well location, obtain image well distance.
- Represent the result in a table

Equations (3.6) and (3.7) are solved for right angle, same object well design, while considering equal distances from the object well, as well as unequal distances. Results are plotted on same axes as type curves for ideal, damaged, and stimulated object well bore. Well bore storage, skin and distance of boundary from object well is also varied. Throughout the computation, $t_D = 10^{-3}\ \text{to}10^{7}$, $c_D = 10^{-3}\text{to}10^{2}$ and $s = 5,10,0, -0.5$.

CHAPTER FOUR

4 RESULTS AND DISCUSSION

4.1 RESULTS

A fault inclined at 45 degrees would result in 8 number of images wells, and therefore the shortest distance between these image wells and the object well would need to be determined to know the influence each image well as on the object well.

A generalized formula of the shortest image to object well distance is generated for each polygon assuming an equal distance "d" from the two inclined sealing faults acting as mirrors. This equal distance has therefore enable a convergence of different regular polygons depending on the angle of inclination. Where Ow symbolizes Object well, W1 is image well one, W2= image well two, D1 is the shortest distance from image well one to object well, likewise for D2, D3 etc.

Quadrilateral: A Square has an interior angle of 90 degrees, three well images with shortest distance from Image well one (W1) to the Object well (Ow) as '2d'. The following are the shortest distances from each image well to the object well.

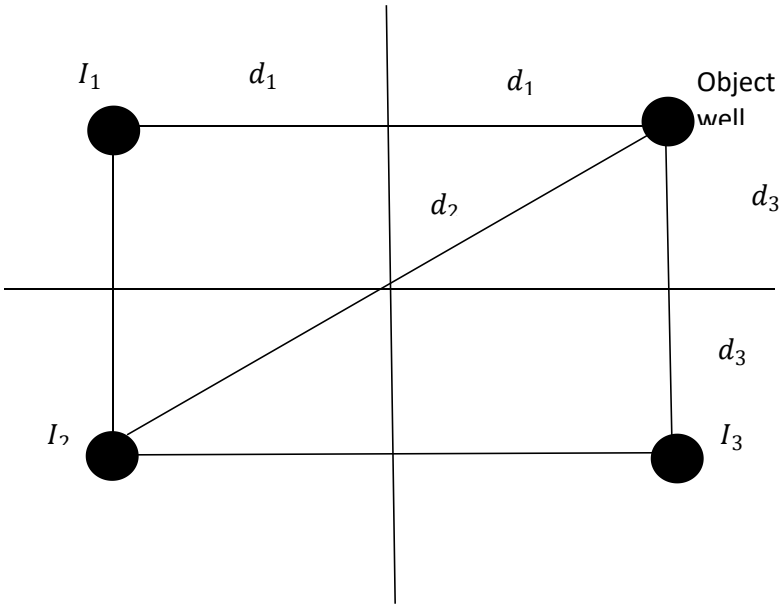

Figure 4.1 Diagram of image well

Comparing the results using different well bore storage, skin and distance of boundary from object well is also varied. Throughout the computation,

$t_D = 10^{-3}\, to 10^7$

$c_D = 10^{-3}, 1, 10, 10^2$ and $s = 10, 0, -0.5$

4.1.1 For comparing close and equal distance to the faults for d_1 and d_3

For $d_1 = 2, d_3 = 2$

$d_2 = \sqrt{2(2)^2 + 2(2)^2} = 2.83$

Where

$$I_1 = 2d_1 = 4$$

$$I_3 = 2d_3 = 4$$

$$I_3 = \sqrt{2{d_1}^2 + 2{d_3}^2} = 2d_2 = 5.66$$

Where I_1 and I_2 are I_3 are the image wells

Dimensionless pressure across the well

$$P_{DOW} = -\frac{1}{2}Ei\left[\frac{r_D^2}{\frac{4t_D}{C_D}}\right] + s - \frac{1}{2}Ei\left[\frac{{I_1}^2}{4t_D}\right] - \frac{1}{2}Ei\left[\frac{{I_2}^2}{4t_D}\right] - \frac{1}{2}Ei\left[\frac{{I_3}^2}{4t_D}\right] + 2s$$

$$P_{DOW} = -\frac{1}{2}Ei\left[\frac{r_D^2}{\frac{4t_D}{C_D}}\right] + s - \frac{1}{2}Ei\left[\frac{4^2}{4t_D}\right] - \frac{1}{2}Ei\left[\frac{5.66^2}{4t_D}\right] - \frac{1}{2}Ei\left[\frac{4^2}{4t_D}\right] + 2s$$

- For $c_D = 10^{-3}$ $s = 10, 0, -0.5$

Table 4.1 At skin of 0

t_D	P_{DOW}	$\frac{dP_{DOW}}{dt_D}$	P'_{DOW}
0.001	0.522141	4.604	0.3894
0.01	1.568254	4.604	0.487655
0.1	2.708378	4.604	0.498797
1	4.102301	4.604	0.935272
10	7.443516	4.604	1.814099
100	11.87574	4.604	1.980137
1000	16.46298	4.604	1.998
10000	21.06634	4.604	1.9998

100000	25.67133	4.604	1.99998
1000000	30.27649	4.604	1.999998
10000000	34.88166	4.604	2
1E+08	39.48683	4.604	2
1E+09	44.092	4.604	2
1E+10	48.69717	4.604	2

Table 4.2 At skin of 10

t_D	P_{DOW}	$\frac{dP_{DOW}}{dt_D}$	P'_{DOW}
0.001	10.52214	4.604	0.3894
0.01	11.56825	4.604	0.487655
0.1	12.70838	4.604	0.498797
1	14.1023	4.604	0.935272
10	17.44352	4.604	1.814099
100	21.87574	4.604	1.980137
1000	26.46298	4.604	1.998
10000	31.06634	4.604	1.9998
100000	35.67133	4.604	1.99998
1000000	40.27649	4.604	1.999998
10000000	44.88166	4.604	2
1E+08	49.48683	4.604	2
1E+09	54.092	4.604	2
1E+10	58.69717	4.604	2

Table 4.3 At skin of -0.5

t_D	P_{DOW}	$\frac{dP_{DOW}}{dt_D}$	P'_{DOW}
0.001	0.022141	4.604	0.3894
0.01	1.068254	4.604	0.487655
0.1	2.208378	4.604	0.498797
1	3.602301	4.604	0.935272
10	6.943516	4.604	1.814099
100	11.37574	4.604	1.980137
1000	15.96298	4.604	1.998
10000	20.56634	4.604	1.9998
100000	25.17133	4.604	1.99998
1000000	29.77649	4.604	1.999998
10000000	34.38166	4.604	2
1E+08	38.98683	4.604	2
1E+09	43.592	4.604	2
1E+10	48.19717	4.604	2

- For $c_D = 1 \quad s = 5,10,0,-0.5$

Table 4.4 At skin of 0

t_D	P_{DOW}	$\frac{dP_{DOW}}{dt_D}$	P'_{DOW}
0.001	0.00	4.604	1.3E-109
0.01	0.00	4.604	6.94E-12
0.1	0.01	4.604	0.041088
1	0.77	4.604	0.824797
10	4.00	4.604	1.801767
100	8.42	4.604	1.97889
1000	13.01	4.604	1.997875
10000	17.61	4.604	1.999787
100000	22.22	4.604	1.999979
1000000	26.82	4.604	1.999998
10000000	31.43	4.604	2
1E+08	36.03	4.604	2
1E+09	40.64	4.604	2
1E+10	45.24	4.604	2

Table 4.5 At skin of 10

t_D	P_{DOW}	$\frac{dP_{DOW}}{dt_D}$	P'_{DOW}
0.001	10	4.604	0.041042
0.01	10	4.604	0.3894
0.1	10.01246	4.604	0.4877
1	10.7659	4.604	0.934148
10	14.00205	4.604	1.813987
100	18.42311	4.604	1.980126
1000	23.00922	4.604	1.997999
10000	27.61248	4.604	1.9998
100000	32.21746	4.604	1.99998
1000000	36.82261	4.604	1.999998
10000000	41.42778	4.604	2
1E+08	46.03295	4.604	2
1E+09	50.63812	4.604	2

1E+10	55.24329	4.604	2

Table 4.6 At skin of -0.5

t_D	P_{DOW}	$\frac{dP_{DOW}}{dt_D}$	P'_{DOW}
0.001	-0.5	4.604	0.041042
0.01	-0.5	4.604	0.3894
0.1	-0.48754	4.604	0.4877
1	0.2659	4.604	0.934148
10	3.502048	4.604	1.813987
100	7.923112	4.604	1.980126
1000	12.50922	4.604	1.997999
10000	17.11248	4.604	1.9998
100000	21.71746	4.604	1.99998
1000000	26.32261	4.604	1.999998
10000000	30.92778	4.604	2
1E+08	35.53295	4.604	2
1E+09	40.13812	4.604	2
1E+10	44.74329	4.604	2

- For $c_D = 10 \quad s = 10{,}0, -0.5$

Table 4.7 At skin of 0

t_D	P_{DOW}	$\frac{dP_{DOW}}{dt_D}$	P'_{DOW}
0.001	0	4.604	0
0.01	0	4.604	0
0.1	0	4.604	0
1	0.256216	4.604	0.476439
10	2.955935	4.604	1.703512
100	7.282993	4.604	1.967793
1000	11.85905	4.604	1.996752
10000	16.4613	4.604	1.999675
100000	21.06618	4.604	1.999967
1000000	25.67132	4.604	1.999997

10000000	30.27649	4.604	2
1E+08	34.88166	4.604	2
1E+09	39.48683	4.604	2
1E+10	44.092	4.604	2

Table 4.8 At skin of 10

t_D	P_{DOW}	$\frac{dP_{DOW}}{dt_D}$	P'_{DOW}
0.001	10	4.604	0
0.01	10	4.604	0
0.1	10.00308	4.604	0.013662
1	10.48695	4.604	0.591358
10	13.31926	4.604	1.722483
100	17.66393	4.604	1.969812
1000	22.24181	4.604	1.996955
10000	26.84424	4.604	1.999695
100000	31.44914	4.604	1.99997
1000000	36.05428	4.604	1.999997
10000000	40.65945	4.604	2
1E+08	45.26462	4.604	2
1E+09	49.86979	4.604	2
1E+10	54.47496	4.604	2

Table 4.9 At skin of -0.5

t_D	P_{DOW}	$\frac{dP_{DOW}}{dt_D}$	P'_{DOW}
0.001	-0.5	4.604	0
0.01	-0.5	4.604	0
0.1	-0.5	4.604	0
1	-0.24378	4.604	0.476439
10	2.455935	4.604	1.703512
100	6.782993	4.604	1.967793
1000	11.35905	4.604	1.996752
10000	15.9613	4.604	1.999675
100000	20.56618	4.604	1.999967
1000000	25.17132	4.604	1.999997
10000000	29.77649	4.604	2
1E+08	34.38166	4.604	2
1E+09	38.98683	4.604	2

1E+10	43.592	4.604	2

❖ **Graph of skin against P_{DOW} for all the different cd**

- Table 4.10 Dimensionless pressure for skin -0.5 at different cd

t_D	cd= 0.001	cd=1	cd=10
	P_{DOW}	P_{DOW}	P_{DOW}
0.001	0.022141	-0.5	-0.5
0.01	1.068254	-0.5	-0.5
0.1	2.208378	-0.48754	-0.5
1	3.602301	0.2659	-0.24378
10	6.943516	3.502048	2.455935
100	11.37574	7.923112	6.782993
1000	15.96298	12.50922	11.35905
10000	20.56634	17.11248	15.9613
100000	25.17133	21.71746	20.56618
1000000	29.77649	26.32261	25.17132
10000000	34.38166	30.92778	29.77649
1E+08	38.98683	35.53295	34.38166
1E+09	43.592	40.13812	38.98683
1E+10	48.19717	44.74329	43.592

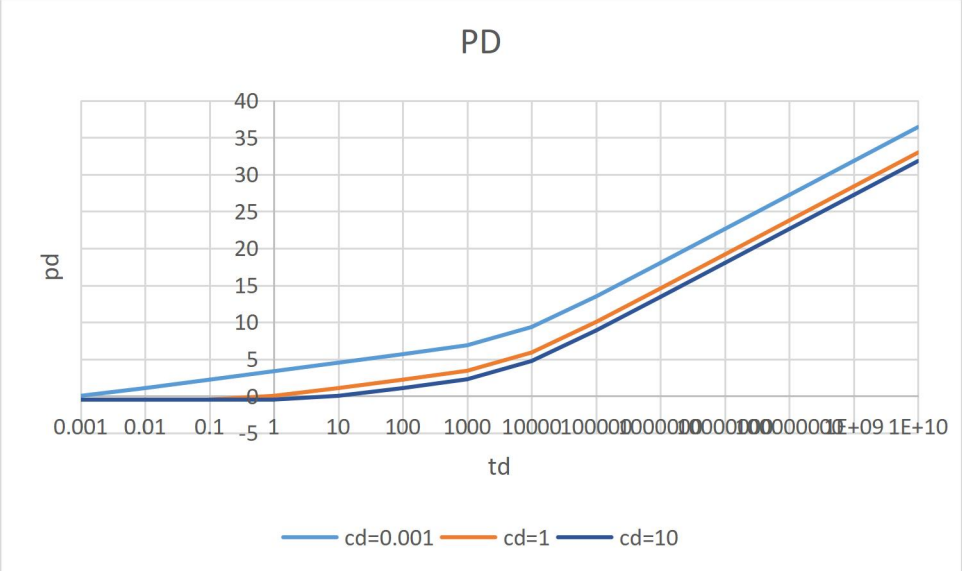

Figure 4.2 Graph of Dimensionless pressure against dimensionless time

- Table 4.11 Dimensionless pressure for skin -0.5 at different cd

t_D	cd= 0.001	cd=1	cd=10
	P_{DOW}	P_{DOW}	P_{DOW}
0.001	0.522141	0	0
0.01	1.568254	0	0
0.1	2.708374	0.01	0
1	3.858542	0.77	0.256216
10	5.009722	4	2.955935
100	6.161003	8.42	7.282993
1000	7.367922	13.01	11.85905
10000	9.84039	17.61	16.4613
100000	13.97271	22.22	21.06618
1000000	18.5235	26.82	25.67132
10000000	23.12315	31.43	30.27649
1E+08	27.72776	36.03	34.88166
1E+09	32.33288	40.64	39.48683
1E+10	36.93804	45.24	44.092

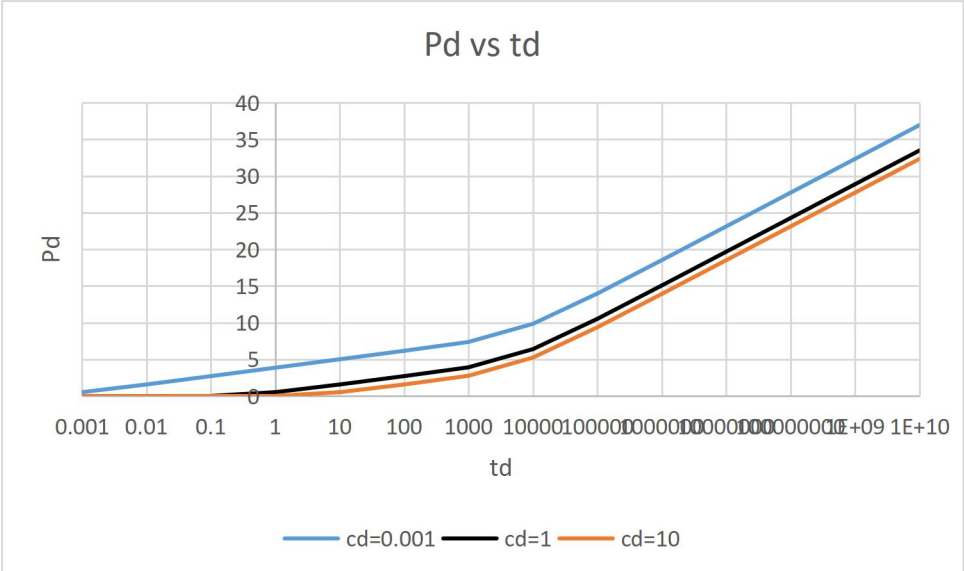

Figure 4.3 Graph of Dimensionless pressure against dimensionless time

- Table 4.12 Dimensionless pressure for skin 10 at different cd

t_D	cd= 0.001	cd=1	cd=10
	P_{DOW}	P_{DOW}	P_{DOW}
0.001	10.52214	10	10
0.01	11.56825	10	10
0.1	12.70837	10.01246	10.00308
1	13.85854	10.7659	10.48695
10	15.00972	14.00205	13.31926
100	16.161	18.42311	17.66393
1000	17.36792	23.00922	22.24181
10000	19.84039	27.61248	26.84424
100000	23.97271	32.21746	31.44914
1000000	28.5235	36.82261	36.05428
10000000	33.12315	41.42778	40.65945
1E+08	37.72776	46.03295	45.26462
1E+09	42.33288	50.63812	49.86979
1E+10	46.93804	55.24329	54.47496

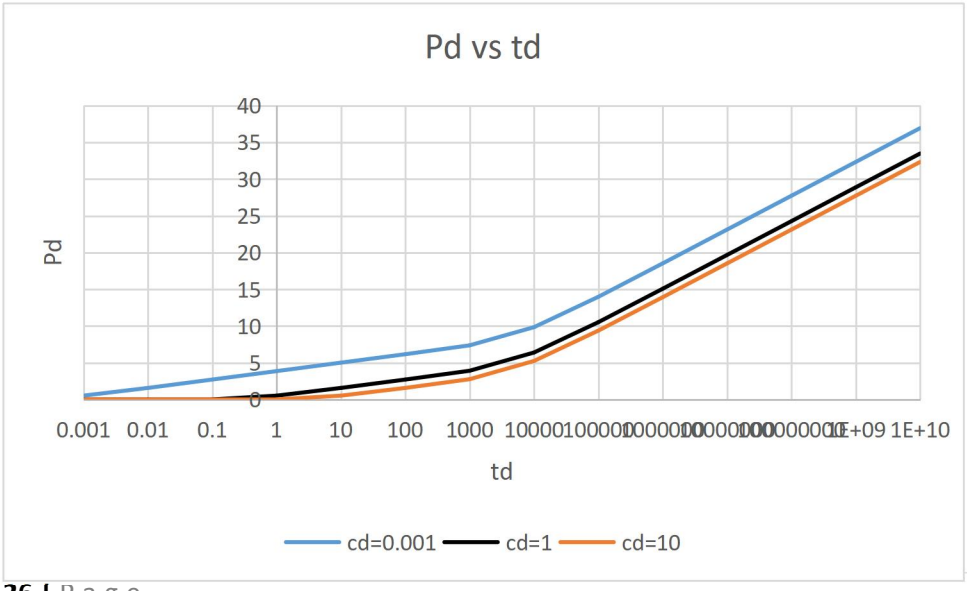

Figure 4.4 Graph of Dimensionless pressure against dimensionless time

❖ **Graph of skin against P'_{DOW} for all the different cd**

- Table 4.13 Dimensionless pressure derivative for skin -0.5 at different cd

t_D	cd=0.001	cd=1	cd =10
	P'_{DOW}	P'_{DOW}	P'_{DOW}
0.001	0.00	0.00	0.00
0.01	0.00	0.00	0.00
0.1	0.00	0.00	0.00
1	0.04	0.04	0.04
10	0.39	0.39	0.39
100	0.49	0.49	0.49
1000	0.58	0.58	0.58
10000	1.46	1.46	1.46
100000	1.93	1.93	1.93
1000000	1.99	1.99	1.99
10000000	2.00	2.00	2.00
1E+08	2.00	2.00	2.00
1E+09	2.00	2.00	2.00
1E+10	2.00	2.00	2.00

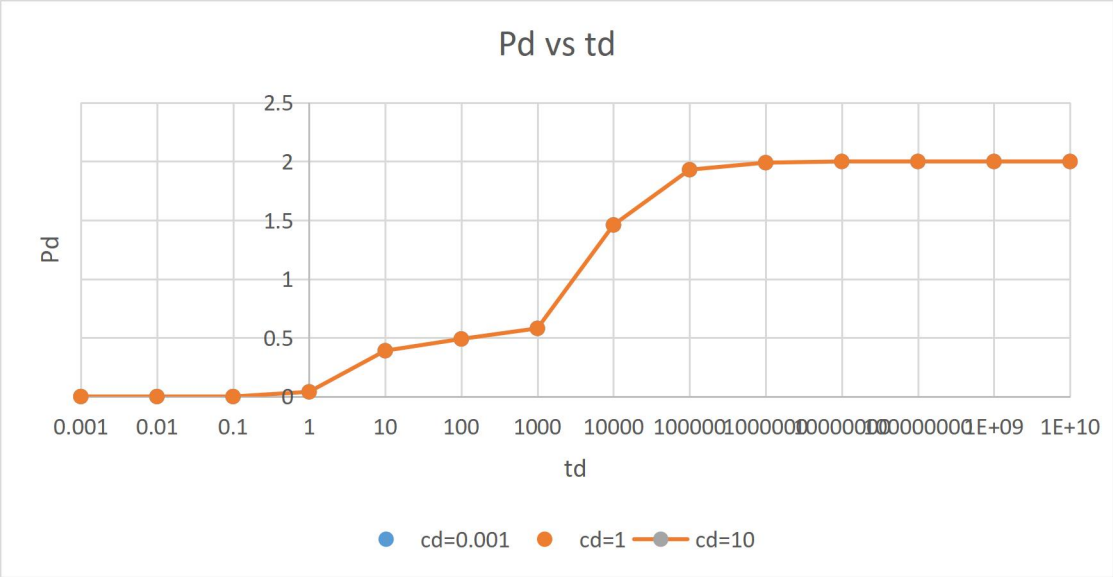

Figure 4.5 Graph of Dimensionless pressure derivative against dimensionless time

- Table 4.14 Dimensionless pressure derivative for skin 0 at different cd

t_D	cd=0.001	cd=1	cd =10
	P'_{DOW}	P'_{DOW}	P'_{DOW}
0.001	0.00	0.00	0.00
0.01	0.00	0.00	0.00
0.1	0.00	0.00	0.00
1	0.04	0.04	0.04
10	0.39	0.39	0.39
100	0.49	0.49	0.49
1000	0.58	0.58	0.58
10000	1.46	1.46	1.46
100000	1.93	1.93	1.93
1000000	1.99	1.99	1.99
10000000	2.00	2.00	2.00
1E+08	2.00	2.00	2.00
1E+09	2.00	2.00	2.00
1E+10	2.00	2.00	2.00

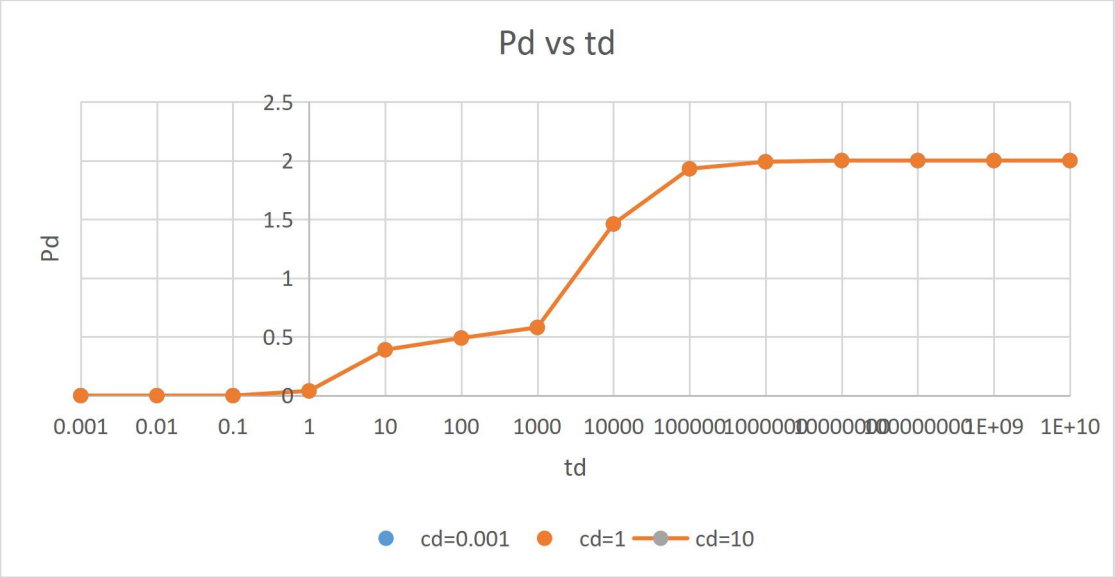

Figure 4.6 Graph of Dimensionless pressure dervative against dimensionless time

- Table 4.15 Dimensionless pressure derivative for skin 10 at different cd

t_D	cd=0.001	cd=1	cd =10
	P'_{DOW}	P'_{DOW}	P'_{DOW}
0.001	0.00	0.00	0.00
0.01	0.00	0.00	0.00
0.1	0.00	0.00	0.00
1	0.04	0.04	0.04
10	0.39	0.39	0.39
100	0.49	0.49	0.49
1000	0.58	0.58	0.58
10000	1.46	1.46	1.46
100000	1.93	1.93	1.93
1000000	1.99	1.99	1.99
10000000	2.00	2.00	2.00
1E+08	2.00	2.00	2.00
1E+09	2.00	2.00	2.00
1E+10	2.00	2.00	2.00

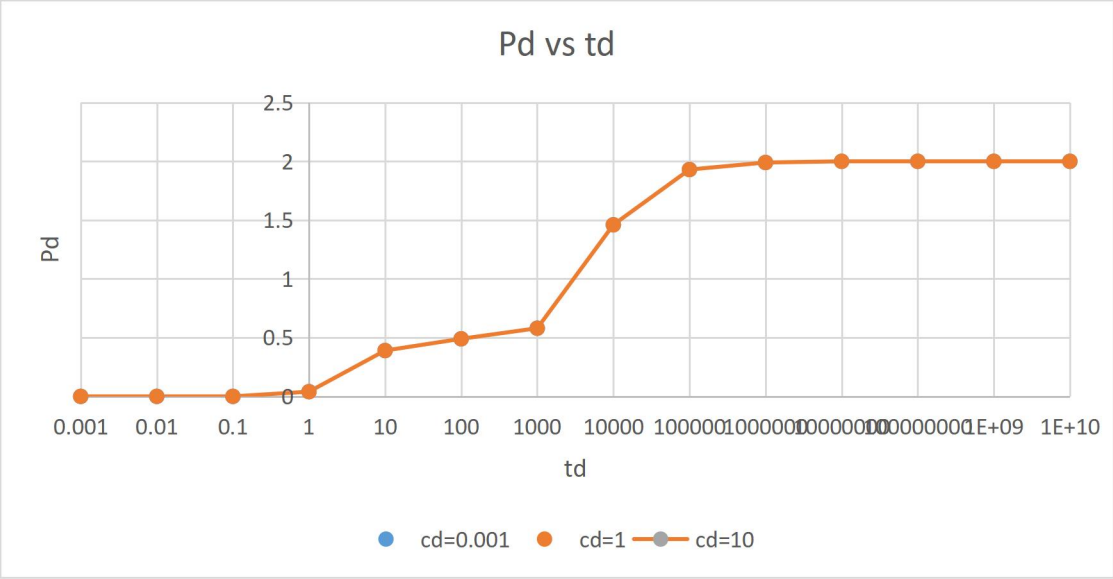

Figure 4.7 Graph of Dimensionless pressure derivatives against dimensionless time

4.1.2 For comparing close and different distance to the faults for d_1 and d_3

For $d_1 = 2, d_3 = 1.2$

$d_2 = \sqrt{2(2)^2 + 2(1.2)^2} = 2.83$

where

$$I_1 = 2d_1 = 4$$

$$I_3 = 2d_3 = 1.44$$

$$I_3 = \sqrt{2{d_1}^2 + 2{d_3}^2} = 2d_2 = 6.69$$

Where I_1 and I_2 are I_3 are the image wells

Dimensionless pressure across the well

$$P_{DOW} = -\frac{1}{2}Ei\left[\frac{r_D^2}{\frac{4t_D}{C_D}}\right] + s - \frac{1}{2}Ei\left[\frac{{I_1}^2}{4t_D}\right] - \frac{1}{2}Ei\left[\frac{{I_2}^2}{4t_D}\right] - \frac{1}{2}Ei\left[\frac{{I_3}^2}{4t_D}\right] + 2s$$

$$P_{DOW} = -\frac{1}{2}Ei\left[\frac{r_D^2}{\frac{4t_D}{C_D}}\right] + s - \frac{1}{2}Ei\left[\frac{4^2}{4t_D}\right] - \frac{1}{2}Ei\left[\frac{6.69^2}{4t_D}\right] - \frac{1}{2}Ei\left[\frac{1.44^2}{4t_D}\right] + 2s$$

- For $c_D = 10^{-3}$ $s = 5,10,0,-0.5$

Table 4.16 At skin of 0

t_D	P_{DOW}	$\frac{dP_{DOW}}{dt_D}$	P'_{DOW}
0.001	0.522141	4.604	0.3894
0.01	1.568254	4.604	0.487655
0.1	2.711456	4.604	0.512436
1	4.36478	4.604	1.065508
10	7.801836	4.604	1.815558
100	12.23329	4.604	1.979798
1000	16.8202	4.604	1.997961
10000	21.42353	4.604	1.999796
100000	26.02852	4.604	1.99998
1000000	30.63367	4.604	1.999998
10000000	35.23884	4.604	2
1E+08	39.84401	4.604	2
1E+09	44.44918	4.604	2
1E+10	49.05435	4.604	2

Table 4.17 At skin of 10

t_D	P_{DOW}	$\frac{dP_{DOW}}{dt_D}$	P'_{DOW}
0.001	10.52214	4.604	0.3894
0.01	11.56825	4.604	0.487655
0.1	12.71146	4.604	0.512436
1	14.36478	4.604	1.065508
10	17.80184	4.604	1.815558
100	22.23329	4.604	1.979798
1000	26.8202	4.604	1.997961
10000	31.42353	4.604	1.999796
100000	36.02852	4.604	1.99998
1000000	40.63367	4.604	1.999998
10000000	45.23884	4.604	2
1E+08	49.84401	4.604	2
1E+09	54.44918	4.604	2
1E+10	59.05435	4.604	2

Table 4.18 At skin of -0.5

t_D	P_{DOW}	$\frac{dP_{DOW}}{dt_D}$	P'_{DOW}
0.001	0.022141	4.604	0.3894
0.01	1.068254	4.604	0.487655
0.1	2.211456	4.604	0.512436
1	3.86478	4.604	1.065508
10	7.301836	4.604	1.815558
100	11.73329	4.604	1.979798
1000	16.3202	4.604	1.997961
10000	20.92353	4.604	1.999796
100000	25.52852	4.604	1.99998
1000000	30.13367	4.604	1.999998
10000000	34.73884	4.604	2
1E+08	39.34401	4.604	2
1E+09	43.94918	4.604	2
1E+10	48.55435	4.604	2

- For $c_D = 1 \quad s = 5,10,0,-0.5$

Table 4.19 At skin of 0

t_D	P_{DOW}	$\frac{dP_{DOW}}{dt_D}$	P'_{DOW}
0.001	0.00	4.604	1.3E-109
0.01	0.00	4.604	6.94E-12
0.1	0.01	4.604	0.041088
1	0.77	4.604	0.824797
10	4.00	4.604	1.801767
100	8.42	4.604	1.97889
1000	13.01	4.604	1.997875
10000	17.61	4.604	1.999787
100000	22.22	4.604	1.999979
1000000	26.82	4.604	1.999998
10000000	31.43	4.604	2
1E+08	36.03	4.604	2
1E+09	40.64	4.604	2
1E+10	45.24	4.604	2

Table 4.20 At skin of 10

t_D	P_{DOW}	$\frac{dP_{DOW}}{dt_D}$	P'_{DOW}
0.001	10	4.604	0.041042
0.01	10	4.604	0.3894
0.1	10.01246	4.604	0.4877
1	10.7659	4.604	0.934148
10	14.00205	4.604	1.813987
100	18.42311	4.604	1.980126
1000	23.00922	4.604	1.997999
10000	27.61248	4.604	1.9998
100000	32.21746	4.604	1.99998
1000000	36.82261	4.604	1.999998
10000000	41.42778	4.604	2
1E+08	46.03295	4.604	2
1E+09	50.63812	4.604	2
1E+10	55.24329	4.604	2

Table 4.21 At skin of -0.5

t_D	P_{DOW}	$\frac{dP_{DOW}}{dt_D}$	P'_{DOW}
0.001	-0.5	4.604	0.041042
0.01	-0.5	4.604	0.3894
0.1	-0.48754	4.604	0.4877
1	0.2659	4.604	0.934148
10	3.502048	4.604	1.813987
100	7.923112	4.604	1.980126
1000	12.50922	4.604	1.997999
10000	17.11248	4.604	1.9998
100000	21.71746	4.604	1.99998
1000000	26.32261	4.604	1.999998
10000000	30.92778	4.604	2
1E+08	35.53295	4.604	2
1E+09	40.13812	4.604	2
1E+10	44.74329	4.604	2

- For $c_D = 10 \quad s = 5,10,0,-0.5$

Table 4.22At skin of 0

t_D	P_{DOW}	$\frac{dP_{DOW}}{dt_D}$	P'_{DOW}
0.001	0.00	4.604	0.00
0.01	0.00	4.604	0.00
0.1	0.00	4.604	0.01
1	0.52	4.604	0.61
10	3.31	4.604	1.70
100	7.64	4.604	1.97
1000	12.22	4.604	2.00
10000	16.82	4.604	2.00
100000	21.42	4.604	2.00
1000000	26.03	4.604	2.00
10000000	30.63	4.604	2.00
1E+08	35.24	4.604	2.00
1E+09	39.84	4.604	2.00
1E+10	44.45	4.604	2.00

Table 4.23 At skin of 10

t_D	P_{DOW}	$\frac{dP_{DOW}}{dt_D}$	P'_{DOW}
0.001	10	4.604	0.00
0.01	10	4.604	0.00
0.1	10.00308	4.604	0.01
1	10.5187	4.604	0.61
10	13.31426	4.604	1.70
100	17.64054	4.604	1.97
1000	22.21627	4.604	2.00
10000	26.81848	4.604	2.00
100000	31.42336	4.604	2.00
1000000	36.0285	4.604	2.00
10000000	40.63367	4.604	2.00
1E+08	45.23884	4.604	2.00
1E+09	49.84401	4.604	2.00
1E+10	54.44918	4.604	2.00

Table 4.24 At skin of -0.5

t_D	P_{DOW}	$\frac{dP_{DOW}}{dt_D}$	P'_{DOW}
0.001	-0.5	4.604	0.00
0.01	-0.5	4.604	0.00
0.1	-0.49692	4.604	0.01
1	0.018696	4.604	0.61
10	2.814255	4.604	1.70
100	7.140543	4.604	1.97
1000	11.71627	4.604	2.00
10000	16.31848	4.604	2.00
100000	20.92336	4.604	2.00
1000000	25.5285	4.604	2.00
10000000	30.13367	4.604	2.00
1E+08	34.73884	4.604	2.00
1E+09	39.34401	4.604	2.00
1E+10	43.94918	4.604	2.00

❖ Graph of skin against P_{DOW} for all the different cd

- Table 4.25 Dimensionless pressure for skin -0.5 at different cd

t_D	cd= 0.001	cd=1	cd=10
	P_{DOW}	P_{DOW}	P_{DOW}
0.001	0.022141	-0.5	-0.5
0.01	1.068254	-0.5	-0.5
0.1	2.211456	-0.48754	-0.49692
1	3.86478	0.2659	0.018696
10	7.301836	3.502048	2.814255
100	11.73329	7.923112	7.140543
1000	16.3202	12.50922	11.71627
10000	20.92353	17.11248	16.31848
100000	25.52852	21.71746	20.92336
1000000	30.13367	26.32261	25.5285
10000000	34.73884	30.92778	30.13367
1E+08	39.34401	35.53295	34.73884
1E+09	43.94918	40.13812	39.34401
1E+10	48.55435	44.74329	43.94918

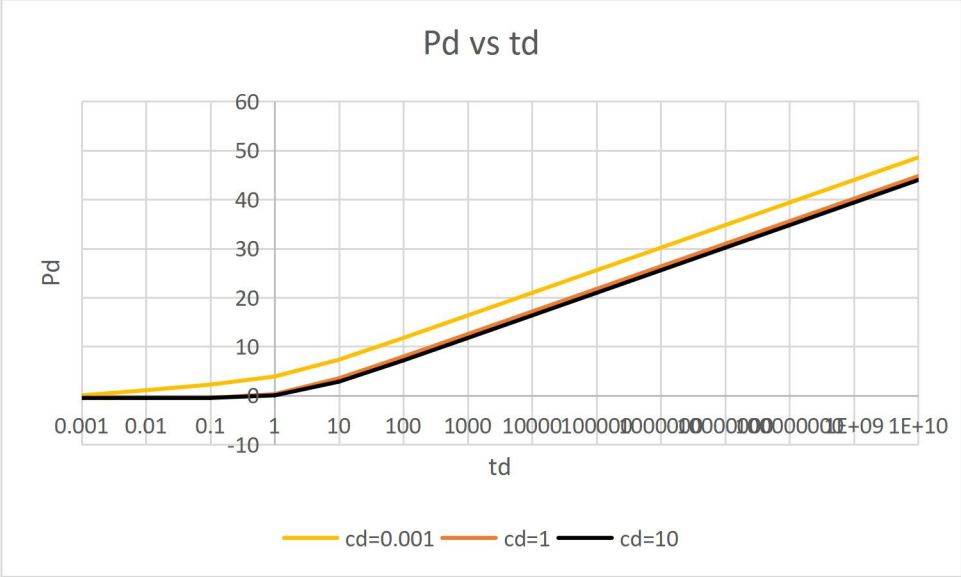

Figure 4.8 Graph of Dimensionless pressure against dimensionless time

- Table 4.26 Dimensionless pressure for skin 0 at different cd

t_D	cd= 0.001	cd=1	cd=10
	P_{DOW}	P_{DOW}	P_{DOW}
0.001	0.522141	0.00	0.00
0.01	1.568254	0.00	0.00
0.1	2.711456	0.01	0.00
1	4.36478	0.77	0.52
10	7.801836	4.00	3.31
100	12.23329	8.42	7.64
1000	16.8202	13.01	12.22
10000	21.42353	17.61	16.82
100000	26.02852	22.22	21.42
1000000	30.63367	26.82	26.03
10000000	35.23884	31.43	30.63
1E+08	39.84401	36.03	35.24
1E+09	44.44918	40.64	39.84
1E+10	49.05435	45.24	44.45

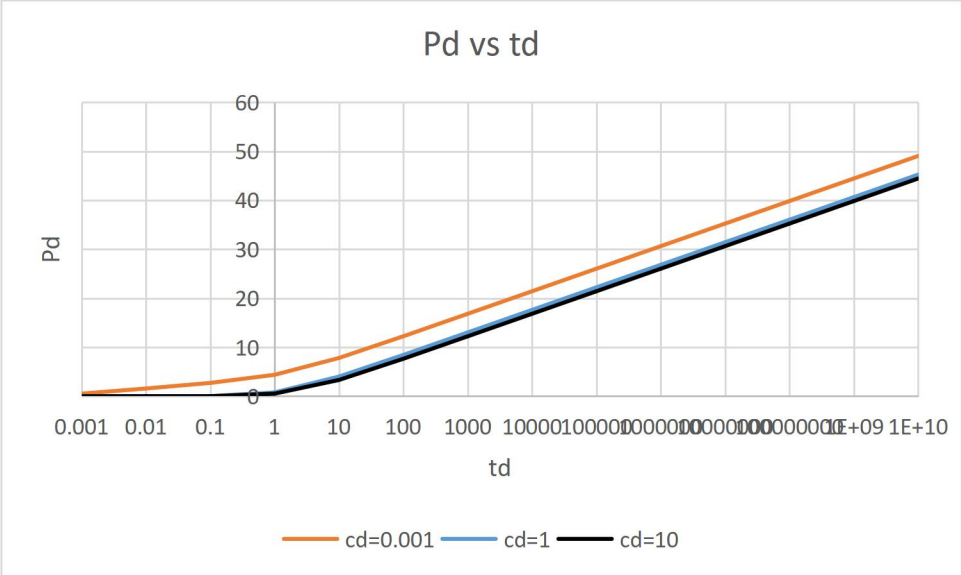

Figure 4.9 Graph of Dimensionless pressure against dimensionless time

- Table 4.27Dimensionless pressure for skin 10 at different cd

t_D	cd= 0.001	cd=1	cd=10
	P_{DOW}	P_{DOW}	P_{DOW}
0.001	10.52214	10	10
0.01	11.56825	10	10
0.1	12.71146	10.01246	10.00308
1	14.36478	10.7659	10.5187
10	17.80184	14.00205	13.31426
100	22.23329	18.42311	17.64054
1000	26.8202	23.00922	22.21627
10000	31.42353	27.61248	26.81848
100000	36.02852	32.21746	31.42336
1000000	40.63367	36.82261	36.0285
10000000	45.23884	41.42778	40.63367
1E+08	49.84401	46.03295	45.23884
1E+09	54.44918	50.63812	49.84401
1E+10	59.05435	55.24329	54.4491

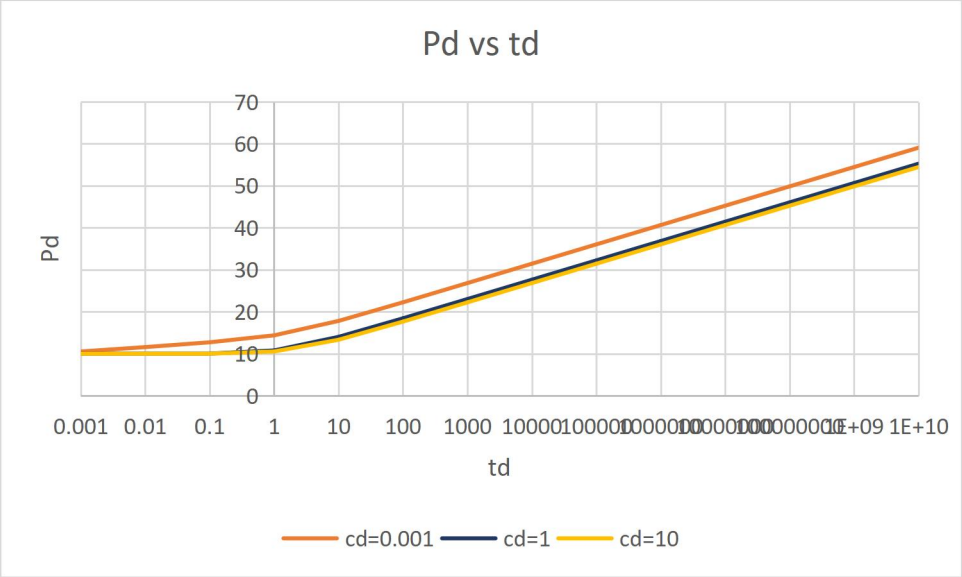

Figure 4.10 Graph of Dimensionless pressure against dimensionless time

❖ Graph of skin against P'_{DOW} for all the different cd

- Table 4.28 Dimensionless pressure derivative for skin -0.5 at different cd

t_D	cd=0.001	cd=1	cd =10
	P'_{DOW}	P'_{DOW}	P'_{DOW}
0.001	0.00	0.00	0.00
0.01	0.00	0.00	0.00
0.1	0.00	0.00	0.00
1	0.04	0.04	0.04
10	0.39	0.39	0.39
100	0.49	0.49	0.49
1000	0.58	0.58	0.58
10000	1.46	1.46	1.46
100000	1.93	1.93	1.93
1000000	1.99	1.99	1.99
10000000	2.00	2.00	2.00
1E+08	2.00	2.00	2.00
1E+09	2.00	2.00	2.00
1E+10	2.00	2.00	2.00

- Table 4.29 Dimensionless pressure derivative for skin 0 at different cd

t_D	cd=0.001	cd=1	cd =10
	P'_{DOW}	P'_{DOW}	P'_{DOW}
0.001	0.00	0.00	0.00
0.01	0.00	0.00	0.00
0.1	0.00	0.00	0.00
1	0.04	0.04	0.04
10	0.39	0.39	0.39
100	0.49	0.49	0.49
1000	0.58	0.58	0.58
10000	1.46	1.46	1.46
100000	1.93	1.93	1.93
1000000	1.99	1.99	1.99
10000000	2.00	2.00	2.00
1E+08	2.00	2.00	2.00
1E+09	2.00	2.00	2.00
1E+10	2.00	2.00	2.00

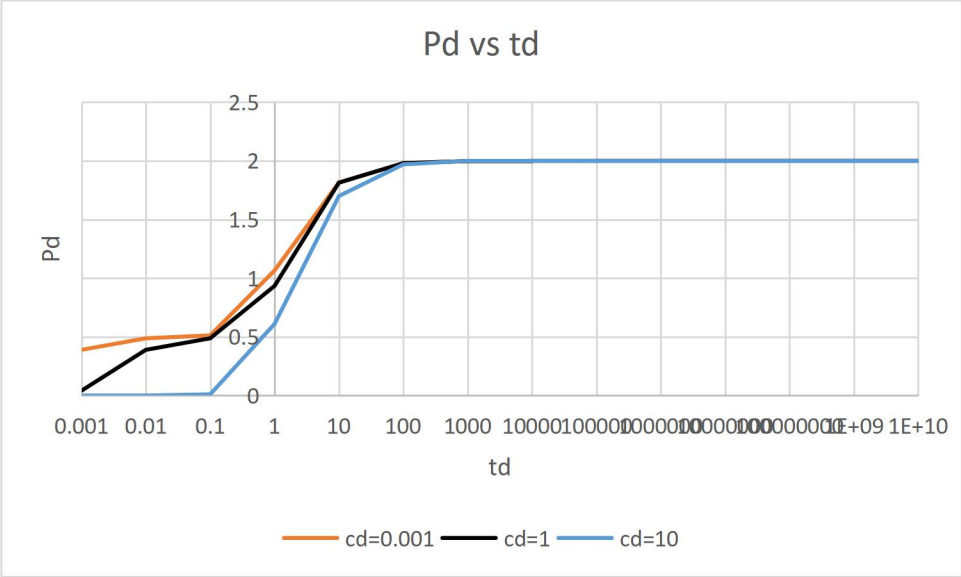

Figure 4.11 Graph of Dimensionless pressure derivative against dimensionless time

- Table 4.30 Dimensionless pressure derivative for skin 10 at different cd

t_D	cd=0.001	cd=1	cd =10
	P'_{DOW}	P'_{DOW}	P'_{DOW}
0.001	0.00	0.00	0.00
0.01	0.00	0.00	0.00
0.1	0.00	0.00	0.00
1	0.04	0.04	0.04
10	0.39	0.39	0.39
100	0.49	0.49	0.49
1000	0.58	0.58	0.58
10000	1.46	1.46	1.46
100000	1.93	1.93	1.93
1000000	1.99	1.99	1.99
10000000	2.00	2.00	2.00
1E+08	2.00	2.00	2.00
1E+09	2.00	2.00	2.00
1E+10	2.00	2.00	2.00

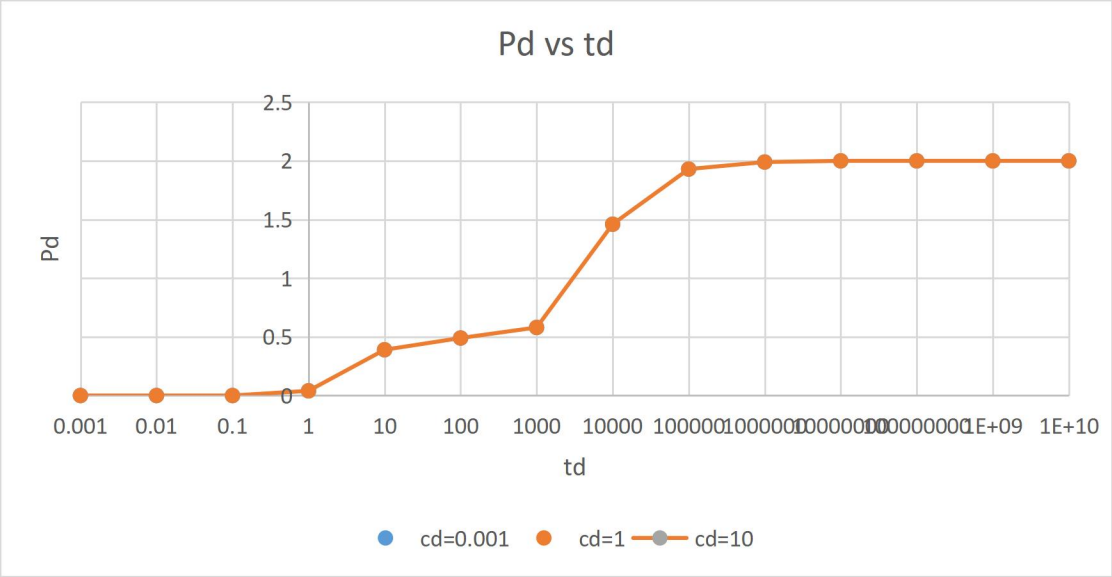

Figure 4.12 Graph of Dimensionless pressure derivatives against dimensionless time

4.1.3 Comparing farther and equal distance to the faults for d_1 and d_3

For $d_1 = 100, d_3 = 100$

$d_2 = \sqrt{2(2)^2 + 2(2)^2} = 2.83$

where

$$I_1 = 2d_1 = 200$$

$$I_3 = 2d_3 = 200$$

$$I_3 = \sqrt{2{d_1}^2 + 2{d_3}^2} = 2d_2 = 400$$

Where I_1 and I_2 are I_3 are the image wells

Dimensionless pressure across the well

$$P_{DOW} = -\frac{1}{2}Ei\left[\frac{r_D^2}{\frac{4t_D}{C_D}}\right] + s - \frac{1}{2}Ei\left[\frac{{I_1}^2}{4t_D}\right] - \frac{1}{2}Ei\left[\frac{{I_2}^2}{4t_D}\right] - \frac{1}{2}Ei\left[\frac{{I_3}^2}{4t_D}\right] + 2s$$

$$P_{DOW} = -\frac{1}{2}Ei\left[\frac{r_D^2}{\frac{4t_D}{C_D}}\right] + s - \frac{1}{2}Ei\left[\frac{200^2}{4t_D}\right] - \frac{1}{2}Ei\left[\frac{400^2}{4t_D}\right] - \frac{1}{2}Ei\left[\frac{200^2}{4t_D}\right] + 2s$$

- For $c_D = 10^{-3} \quad s = 10{,}0{,} -0.5$

Table 4.31 At skin of 0

t_D	P_{DOW}	$\frac{dP_{DOW}}{dt_D}$	P'_{DOW}
0.001	0.522141	4.604	0.3894
0.01	1.568254	4.604	0.487655
0.1	2.708374	4.604	0.498752
1	3.858542	4.604	0.499875
10	5.009722	4.604	0.499988
100	6.161003	4.604	0.499999
1000	7.337212	4.604	0.582108
10000	9.617562	4.604	1.46274
100000	13.66285	4.604	1.927729
1000000	18.20188	4.604	1.992528
10000000	22.80032	4.604	1.99925
1E+08	27.40481	4.604	1.999925
1E+09	32.00992	4.604	1.999993
1E+10	36.61508	4.604	1.999999

Table 4.32 At skin of 10

t_D	P_{DOW}	$\frac{dP_{DOW}}{dt_D}$	P'_{DOW}
0.001	10.52214	4.604	0.3894
0.01	11.56825	4.604	0.487655
0.1	12.70837	4.604	0.498752
1	13.85854	4.604	0.499875
10	15.00972	4.604	0.499988
100	16.161	4.604	0.499999
1000	17.33721	4.604	0.582108
10000	19.61756	4.604	1.46274
100000	23.66285	4.604	1.927729
1000000	28.20188	4.604	1.992528
10000000	32.80032	4.604	1.99925
1E+08	37.40481	4.604	1.999925
1E+09	42.00992	4.604	1.999993
1E+10	46.61508	4.604	1.999999

Table 4.33 At skin of -0.5

t_D	P_{DOW}	$\frac{dP_{DOW}}{dt_D}$	P'_{DOW}
0.001	0.022141	4.604	0.3894
0.01	1.068254	4.604	0.487655
0.1	2.208374	4.604	0.498752
1	3.358542	4.604	0.499875
10	4.509722	4.604	0.499988
100	5.661003	4.604	0.499999
1000	6.837212	4.604	0.582108
10000	9.117562	4.604	1.46274
100000	13.16285	4.604	1.927729
1000000	17.70188	4.604	1.992528
10000000	22.30032	4.604	1.99925
1E+08	26.90481	4.604	1.999925
1E+09	31.50992	4.604	1.999993
1E+10	36.11508	4.604	1.999999

- For $c_D = 1 \quad s = 10{,}0, -0.5$

Table 4.34 At skin of 0

t_D	P_{DOW}	$\frac{dP_{DOW}}{dt_D}$	P'_{DOW}
0.001	0.00	4.604	0.00
0.01	0.00	4.604	0.00
0.1	0.01	4.604	0.04
1	0.52	4.604	0.39
10	1.57	4.604	0.49
100	2.71	4.604	0.50
1000	3.88	4.604	0.58
10000	6.16	4.604	1.46
100000	10.21	4.604	1.93
1000000	14.75	4.604	1.99
10000000	19.35	4.604	2.00
1E+08	23.95	4.604	2.00
1E+09	28.56	4.604	2.00
1E+10	33.16	4.604	2.00

Table 4.35 At skin of 10

t_D	P_{DOW}	$\frac{dP_{DOW}}{dt_D}$	P'_{DOW}
0.001	10	4.604	0.00
0.01	10	4.604	0.00
0.1	10.01246	4.604	0.04
1	10.52214	4.604	0.39
10	11.56825	4.604	0.49
100	12.70837	4.604	0.50
1000	13.88346	4.604	0.58
10000	16.1637	4.604	1.46
100000	20.20897	4.604	1.93
1000000	24.74801	4.604	1.99
10000000	29.34644	4.604	2.00
1E+08	33.95094	4.604	2.00
1E+09	38.55604	4.604	2.00
1E+10	43.1612	4.604	2.00

Table 4.36 At skin of -0.5

t_D	P_{DOW}	$\frac{dP_{DOW}}{dt_D}$	P'_{DOW}
0.001	-0.5	4.604	0.00
0.01	-0.5	4.604	0.00
0.1	-0.48754	4.604	0.04
1	0.022141	4.604	0.39
10	1.068254	4.604	0.49
100	2.208374	4.604	0.50
1000	3.383459	4.604	0.58
10000	5.663697	4.604	1.46
100000	9.708974	4.604	1.93
1000000	14.24801	4.604	1.99
10000000	18.84644	4.604	2.00
1E+08	23.45094	4.604	2.00
1E+09	28.05604	4.604	2.00
1E+10	32.6612	4.604	2.00

- For $c_D = 10 \quad s = 10{,}0, -0.5$

Table 4.37 At skin of 0

t_D	P_{DOW}	$\frac{dP_{DOW}}{dt_D}$	P'_{DOW}
0.001	0.00	4.604	0.00
0.01	0.00	4.604	0.00
0.1	0.00	4.604	0.00
1	0.01	4.604	0.04
10	0.52	4.604	0.39
100	1.57	4.604	0.49
1000	2.73	4.604	0.58
10000	5.01	4.604	1.46
100000	9.06	4.604	1.93
1000000	13.60	4.604	1.99
10000000	18.20	4.604	2.00
1E+08	22.80	4.604	2.00
1E+09	27.40	4.604	2.00
1E+10	32.01	4.604	2.00

Table 4.38 At skin of 10

t_D	P_{DOW}	$\frac{dP_{DOW}}{dt_D}$	P'_{DOW}
0.001	10	4.604	0.00
0.01	10	4.604	0.00
0.1	10	4.604	0.00
1	10.01246	4.604	0.04
10	10.52214	4.604	0.39
100	11.56825	4.604	0.49
1000	12.73329	4.604	0.58
10000	15.01252	4.604	1.46
100000	19.05769	4.604	1.93
1000000	23.59672	4.604	1.99
10000000	28.19515	4.604	2.00
1E+08	32.79964	4.604	2.00
1E+09	37.40475	4.604	2.00
1E+10	42.00991	4.604	2.00

Table 4.39 At skin of -0.5

t_D	P_{DOW}	$\frac{dP_{DOW}}{dt_D}$	P'_{DOW}
0.001	-0.5	4.604	0.00
0.01	-0.5	4.604	0.00
0.1	-0.5	4.604	0.00
1	-0.48754	4.604	0.04
10	0.022141	4.604	0.39
100	1.068254	4.604	0.49
1000	2.233291	4.604	0.58
10000	4.512517	4.604	1.46
100000	8.557692	4.604	1.93
1000000	13.09672	4.604	1.99
10000000	17.69515	4.604	2.00
1E+08	22.29964	4.604	2.00
1E+09	26.90475	4.604	2.00
1E+10	31.50991	4.604	2.00

- ❖ Graph of skin against P_{DOW} for all the different cd

- Table 4.40 Dimensionless pressure for skin -0.5 at different cd

t_D	cd= 0.001	cd=1	cd=10
	P_{DOW}	P_{DOW}	P_{DOW}
0.001	0.022141	-0.5	-0.5
0.01	1.068254	-0.5	-0.5
0.1	2.208374	-0.48754	-0.5
1	3.358542	0.022141	-0.48754
10	4.509722	1.068254	0.022141
100	5.661003	2.208374	1.068254
1000	6.837212	3.383459	2.233291
10000	9.117562	5.663697	4.512517
100000	13.16285	9.708974	8.557692
1000000	17.70188	14.24801	13.09672
10000000	22.30032	18.84644	17.69515
1E+08	26.90481	23.45094	22.29964
1E+09	31.50992	28.05604	26.90475
1E+10	36.11508	32.6612	31.50991

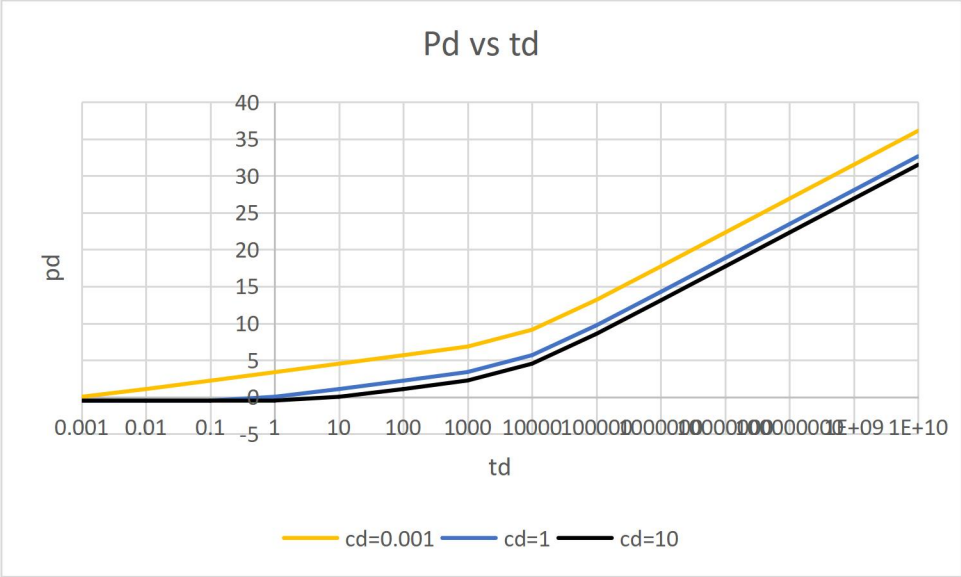

- Table 4.41 Dimensionless pressure for skin 0 at different cd

t_D	cd= 0.001	cd=1	cd=10
	P_{DOW}	P_{DOW}	P_{DOW}
0.001	0.522141	0.00	0.00
0.01	1.568254	0.00	0.00
0.1	2.708374	0.01	0.00
1	3.858542	0.52	0.01
10	5.009722	1.57	0.52
100	6.161003	2.71	1.57
1000	7.337212	3.88	2.73
10000	9.617562	6.16	5.01
100000	13.66285	10.21	9.06
1000000	18.20188	14.75	13.60
10000000	22.80032	19.35	18.20
1E+08	27.40481	23.95	22.80
1E+09	32.00992	28.56	27.40
1E+10	36.61508	33.16	32.01

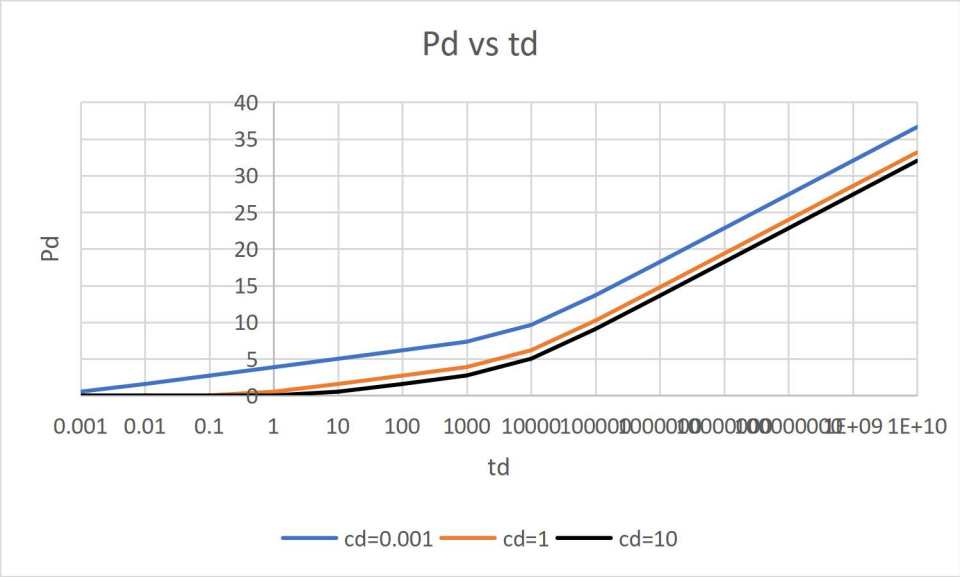

Figure 4.13 Graph of Dimensionless pressure against dimensionless time

- Table 4.42 Dimensionless pressure for skin 10 at different cd

t_D	cd= 0.001	cd=1	cd=10
	P_{DOW}	P_{DOW}	P_{DOW}
0.001	10.52214	10	10
0.01	11.56825	10	10
0.1	12.70837	10.01246	10
1	13.85854	10.52214	10.01246
10	15.00972	11.56825	10.52214
100	16.161	12.70837	11.56825
1000	17.33721	13.88346	12.73329
10000	19.61756	16.1637	15.01252
100000	23.66285	20.20897	19.05769
1000000	28.20188	24.74801	23.59672
10000000	32.80032	29.34644	28.19515
1E+08	37.40481	33.95094	32.79964
1E+09	42.00992	38.55604	37.40475
1E+10	46.61508	43.1612	42.00991

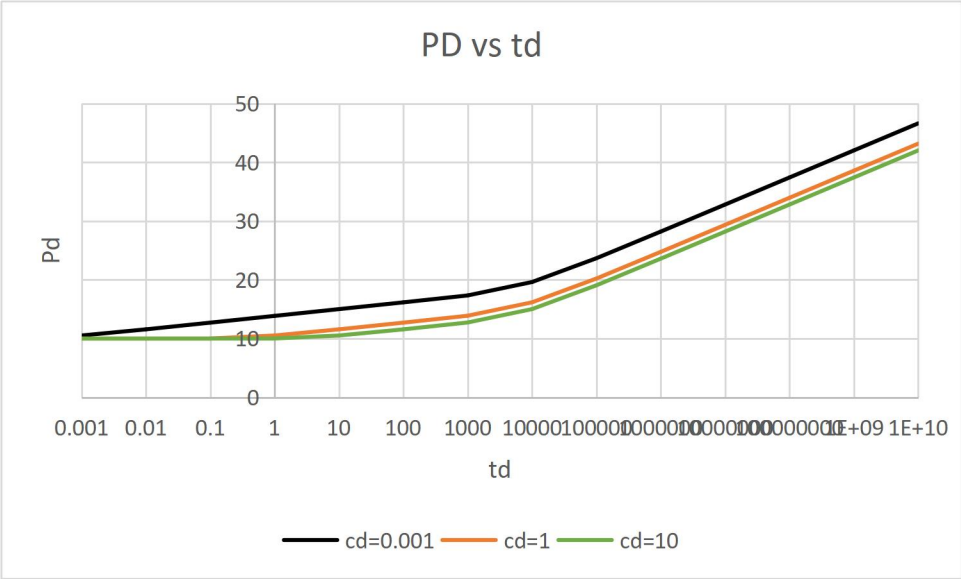

Figure 4.14Graph of Dimensionless pressure against dimensionless time

- ❖ Graph of skin against P'_{DOW} for all the different cd
- Table 4.43 Dimensionless pressure derivative for skin -0.5 at different cd

t_D	cd=0.001	cd=1	cd =10
	P'_{DOW}	P'_{DOW}	P'_{DOW}
0.001	0.00	0.00	0.00
0.01	0.00	0.00	0.00
0.1	0.00	0.00	0.00
1	0.04	0.04	0.04
10	0.39	0.39	0.39
100	0.49	0.49	0.49
1000	0.58	0.58	0.58
10000	1.46	1.46	1.46
100000	1.93	1.93	1.93
1000000	1.99	1.99	1.99
10000000	2.00	2.00	2.00
1E+08	2.00	2.00	2.00
1E+09	2.00	2.00	2.00
1E+10	2.00	2.00	2.00

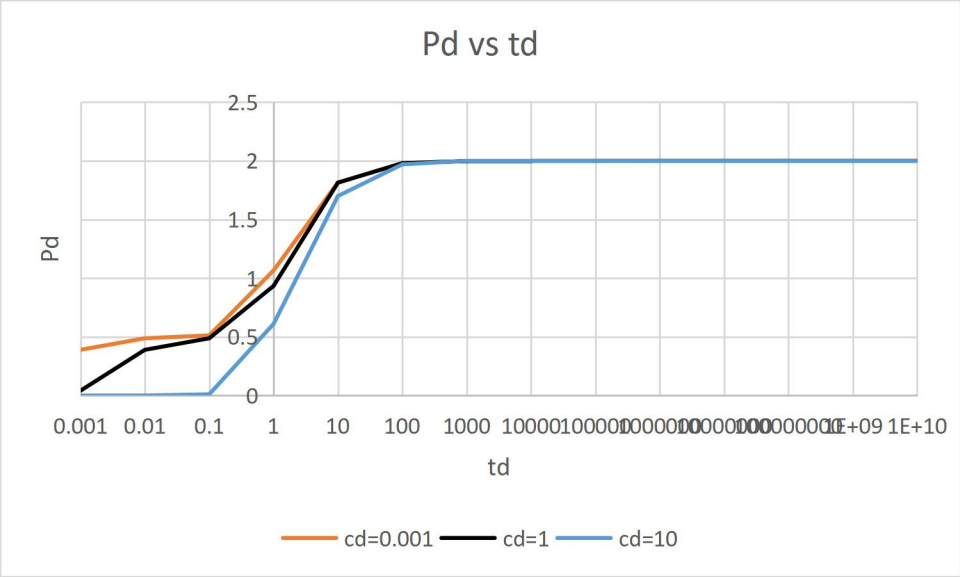

Figure 4.15 Graph of Dimensionless pressure derivative against dimensionless time

- Table 4.44 Dimensionless pressure derivative for skin 0 at different cd

t_D	cd=0.001	cd=1	cd =10
	P'_{DOW}	P'_{DOW}	P'_{DOW}
0.001	0.00	0.00	0.00
0.01	0.00	0.00	0.00
0.1	0.00	0.00	0.00
1	0.04	0.04	0.04
10	0.39	0.39	0.39
100	0.49	0.49	0.49
1000	0.58	0.58	0.58
10000	1.46	1.46	1.46
100000	1.93	1.93	1.93
1000000	1.99	1.99	1.99
10000000	2.00	2.00	2.00
1E+08	2.00	2.00	2.00
1E+09	2.00	2.00	2.00
1E+10	2.00	2.00	2.00

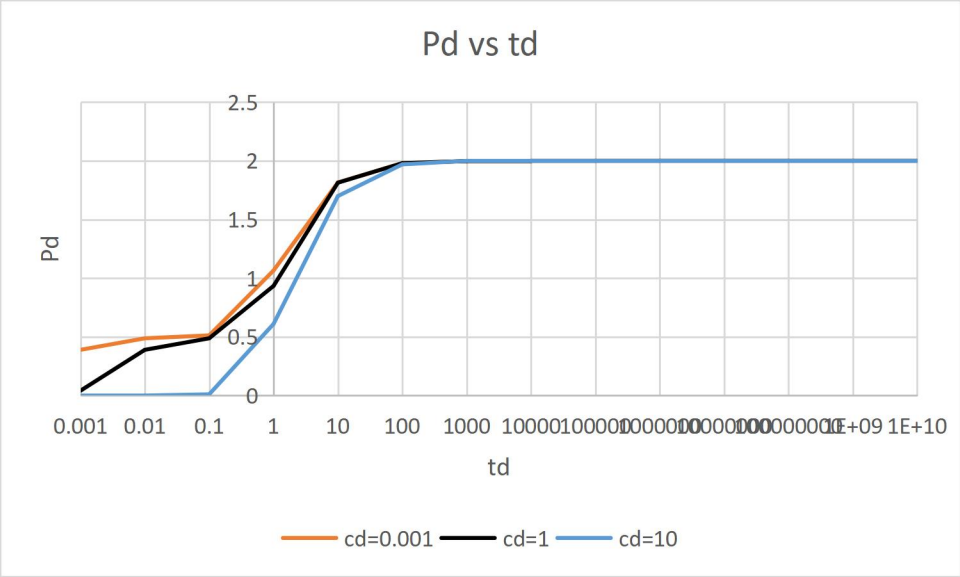

Figure 4.16 Graph of Dimensionless pressure derivatives against dimensionless time

- Table 4.45 Dimensionless pressure derivative for skin 10 at different cd

t_D	cd=0.001	cd=1	cd =10
	P'_{DOW}	P'_{DOW}	P'_{DOW}
0.001	0.00	0.00	0.00
0.01	0.00	0.00	0.00
0.1	0.00	0.00	0.00
1	0.04	0.04	0.04
10	0.39	0.39	0.39
100	0.49	0.49	0.49
1000	0.58	0.58	0.58
10000	1.46	1.46	1.46
100000	1.93	1.93	1.93
1000000	1.99	1.99	1.99
10000000	2.00	2.00	2.00
1E+08	2.00	2.00	2.00
1E+09	2.00	2.00	2.00
1E+10	2.00	2.00	2.00

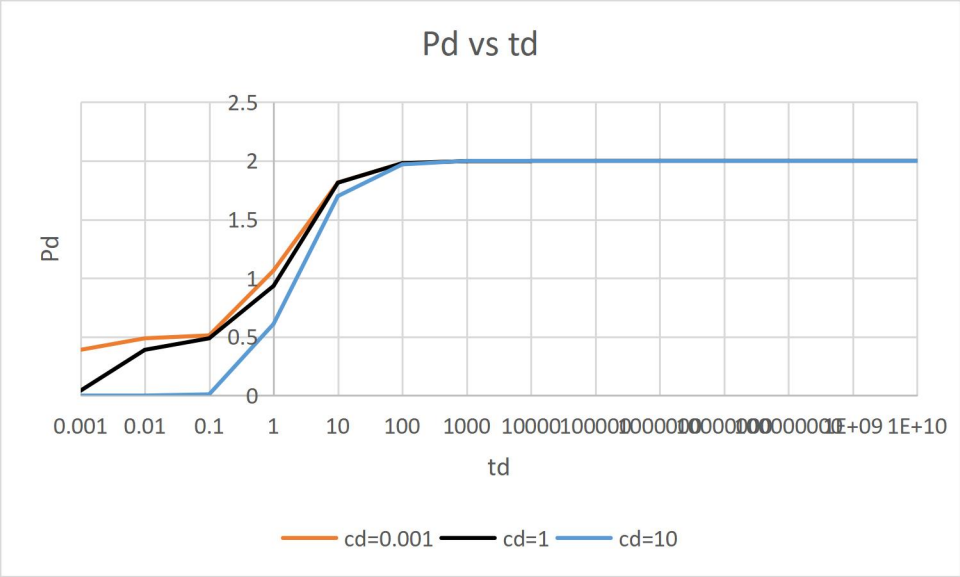

Figure 4.17 Graph of Dimensionless pressure derivative against dimensionless time

4.1.4 Comparing farther and unequal distance to the faults for d_1 and d_3

For $d_1 = 100, d_3 = 80$

$$d_2 = \sqrt{2(2)^2 + 2(2)^2} = 181$$

where

$$I_1 = 2d_1 = 200$$

$$I_3 = 2d_3 = 160$$

$$I_3 = \sqrt{2{d_1}^2 + 2{d_3}^2} = 2d_2 = 362$$

Where I_1 and I_2 are I_3 are the image wells

Dimensionless pressure across the well

$$P_{DOW} = -\frac{1}{2}Ei\left[\frac{r_D^2}{\frac{4t_D}{C_D}}\right] + s - \frac{1}{2}Ei\left[\frac{{I_1}^2}{4t_D}\right] - \frac{1}{2}Ei\left[\frac{{I_2}^2}{4t_D}\right] - \frac{1}{2}Ei\left[\frac{{I_3}^2}{4t_D}\right] + 2s$$

$$P_{DOW} = -\frac{1}{2}\text{Ei}\left[\frac{200^2}{4t_D}\right] - \frac{1}{2}\text{Ei}\left[\frac{362^2}{4t_D}\right] - \frac{1}{2}\text{Ei}\left[\frac{160^2}{4t_D}\right] + 2s$$

- For $c_D = 10^{-3} \quad s = 10{,}0{,} -0.5$

Table 4.46 At skin of 0

t_D	P_{DOW}	$\frac{dP_{DOW}}{dt_D}$	P'_{DOW}
0.001	0.522141	4.604	0.3894
0.01	1.568254	4.604	0.487655
0.1	2.708374	4.604	0.498752
1	3.858542	4.604	0.499875
10	5.009722	4.604	0.499988
100	6.161003	4.604	0.499999
1000	7.367922	4.604	0.642129
10000	9.84039	4.604	1.535903
100000	13.97271	4.604	1.9404
1000000	18.5235	4.604	1.993874
10000000	23.12315	4.604	1.999386
1E+08	27.72776	4.604	1.999939
1E+09	32.33288	4.604	1.999994
1E+10	36.93804	4.604	1.999999

Table 4.47 At skin of 10

t_D	P_{DOW}	$\frac{dP_{DOW}}{dt_D}$	P'_{DOW}
0.001	10.52214	4.604	0.3894
0.01	11.56825	4.604	0.487655
0.1	12.70837	4.604	0.498752
1	13.85854	4.604	0.499875
10	15.00972	4.604	0.499988
100	16.161	4.604	0.499999
1000	17.36792	4.604	0.642129
10000	19.84039	4.604	1.535903
100000	23.97271	4.604	1.9404
1000000	28.5235	4.604	1.993874
10000000	33.12315	4.604	1.999386

1E+08	37.72776	4.604	1.999939
1E+09	42.33288	4.604	1.999994
1E+10	46.93804	4.604	1.999999

Table 4.48 At skin of -0.5

t_D	P_{DOW}	$\frac{dP_{DOW}}{dt_D}$	P'_{DOW}
0.001	0.022141	4.604	0.3894
0.01	1.068254	4.604	0.487655
0.1	2.208374	4.604	0.498752
1	3.358542	4.604	0.499875
10	4.509722	4.604	0.499988
100	5.661003	4.604	0.499999
1000	6.867922	4.604	0.642129
10000	9.34039	4.604	1.535903
100000	13.47271	4.604	1.9404
1000000	18.0235	4.604	1.993874
10000000	22.62315	4.604	1.999386
1E+08	27.22776	4.604	1.999939
1E+09	31.83288	4.604	1.999994
1E+10	36.43804	4.604	1.999999

- For $c_D = 1 \quad s = 10{,}0, -0.5$

Table 4.49 At skin of 0

t_D	P_{DOW}	$\frac{dP_{DOW}}{dt_D}$	P'_{DOW}
0.001	0.00	4.604	0.00
0.01	0.00	4.604	0.00
0.1	0.01	4.604	0.04
1	0.52	4.604	0.39
10	1.57	4.604	0.49
100	2.71	4.604	0.50
1000	3.91	4.604	0.64
10000	6.39	4.604	1.54
100000	10.52	4.604	1.94
1000000	15.07	4.604	1.99
10000000	19.67	4.604	2.00
1E+08	24.27	4.604	2.00
1E+09	28.88	4.604	2.00
1E+10	33.48	4.604	2.00

Table 4.50 At skin of 10

t_D	P_{DOW}	$\frac{dP_{DOW}}{dt_D}$	P'_{DOW}
0.001	10	4.604	0.00
0.01	10	4.604	0.00
0.1	10.01246	4.604	0.04
1	10.52214	4.604	0.39
10	11.56825	4.604	0.49
100	12.70837	4.604	0.50
1000	13.91417	4.604	0.64
10000	16.38652	4.604	1.54
100000	20.51883	4.604	1.94
1000000	25.06962	4.604	1.99
10000000	29.66927	4.604	2.00
1E+08	34.27389	4.604	2.00
1E+09	38.879	4.604	2.00
1E+10	43.48417	4.604	2.00

Table 4.51 At skin of -0.5

t_D	P_{DOW}	$\frac{dP_{DOW}}{dt_D}$	P'_{DOW}
0.001	-0.5	4.604	0.00
0.01	-0.5	4.604	0.00
0.1	-0.48754	4.604	0.04
1	0.022141	4.604	0.39
10	1.068254	4.604	0.49
100	2.208374	4.604	0.50
1000	3.414169	4.604	0.64
10000	5.886524	4.604	1.54
100000	10.01883	4.604	1.94
1000000	14.56962	4.604	1.99
10000000	19.16927	4.604	2.00
1E+08	23.77389	4.604	2.00
1E+09	28.379	4.604	2.00
1E+10	32.98417	4.604	2.00

- For $c_D = 10 \quad s = 10,0,-0.5$

Table 4.52 At skin of 0

t_D	P_{DOW}	$\frac{dP_{DOW}}{dt_D}$	P'_{DOW}
0.001	0.00	4.604	0.00
0.01	0.00	4.604	0.00
0.1	0.00	4.604	0.00
1	0.01	4.604	0.04
10	0.52	4.604	0.39
100	1.57	4.604	0.49
1000	2.76	4.604	0.64
10000	5.24	4.604	1.54
100000	9.37	4.604	1.94
1000000	13.92	4.604	1.99
10000000	18.52	4.604	2.00
1E+08	23.12	4.604	2.00
1E+09	27.73	4.604	2.00
1E+10	32.33	4.604	2.00

Table 4.53 At skin of 10

t_D	P_{DOW}	$\frac{dP_{DOW}}{dt_D}$	P'_{DOW}
0.001	10	4.604	0.00
0.01	10	4.604	0.00
0.1	10	4.604	0.00
1	10.01246	4.604	0.04
10	10.52214	4.604	0.39
100	11.56825	4.604	0.49
1000	12.764	4.604	0.64
10000	15.23534	4.604	1.54
100000	19.36755	4.604	1.94
1000000	23.91833	4.604	1.99
10000000	28.51798	4.604	2.00
1E+08	33.12259	4.604	2.00
1E+09	37.72771	4.604	2.00
1E+10	42.33287	4.604	2.00

Table 4.54 At skin of -0.5

t_D	P_{DOW}	$\frac{dP_{DOW}}{dt_D}$	P'_{DOW}
0.001	-0.5	4.604	0.00
0.01	-0.5	4.604	0.00
0.1	-0.5	4.604	0.00
1	-0.48754	4.604	0.04
10	0.022141	4.604	0.39
100	1.068254	4.604	0.49
1000	2.264001	4.604	0.64
10000	4.735344	4.604	1.54
100000	8.867553	4.604	1.94
1000000	13.41833	4.604	1.99
10000000	18.01798	4.604	2.00
1E+08	22.62259	4.604	2.00
1E+09	27.22771	4.604	2.00
1E+10	31.83287	4.604	2.00

- ❖ Graph of skin against P_{DOW} for all the different cd

- Table 4.55 Dimensionless pressure for skin -0.5 at different cd

t_D	cd= 0.001	cd=1	cd=10
	P_{DOW}	P_{DOW}	P_{DOW}
0.001	0.022141	-0.5	-0.5
0.01	1.068254	-0.5	-0.5
0.1	2.208374	-0.48754	-0.5
1	3.358542	0.022141	-0.48754
10	4.509722	1.068254	0.022141
100	5.661003	2.208374	1.068254
1000	6.867922	3.414169	2.264001
10000	9.34039	5.886524	4.735344
100000	13.47271	10.01883	8.867553
1000000	18.0235	14.56962	13.41833
10000000	22.62315	19.16927	18.01798
1E+08	27.22776	23.77389	22.62259
1E+09	31.83288	28.379	27.22771
1E+10	36.43804	32.98417	31.83287

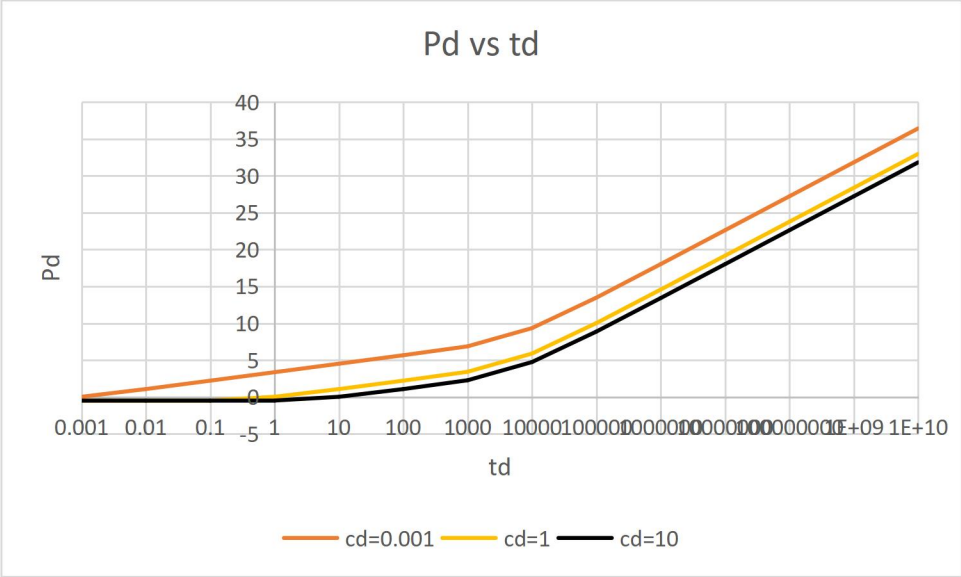

Figure 4.18 Graph of Dimensionless pressure against dimensionless time

- Table 4.56 Dimensionless pressure for skin 0 at different cd

t_D	cd= 0.001	cd=1	cd=10
	P_{DOW}	P_{DOW}	P_{DOW}
0.001	0.522141	0	0
0.01	1.568254	0	0
0.1	2.708374	0.01	0
1	3.858542	0.52	0.01
10	5.009722	1.57	0.52
100	6.161003	2.71	1.57
1000	7.367922	3.91	2.76
10000	9.84039	6.39	5.24
100000	13.97271	10.52	9.37
1000000	18.5235	15.07	13.92
10000000	23.12315	19.67	18.52
1E+08	27.72776	24.27	23.12
1E+09	32.33288	28.88	27.73
1E+10	36.93804	33.48	32.33

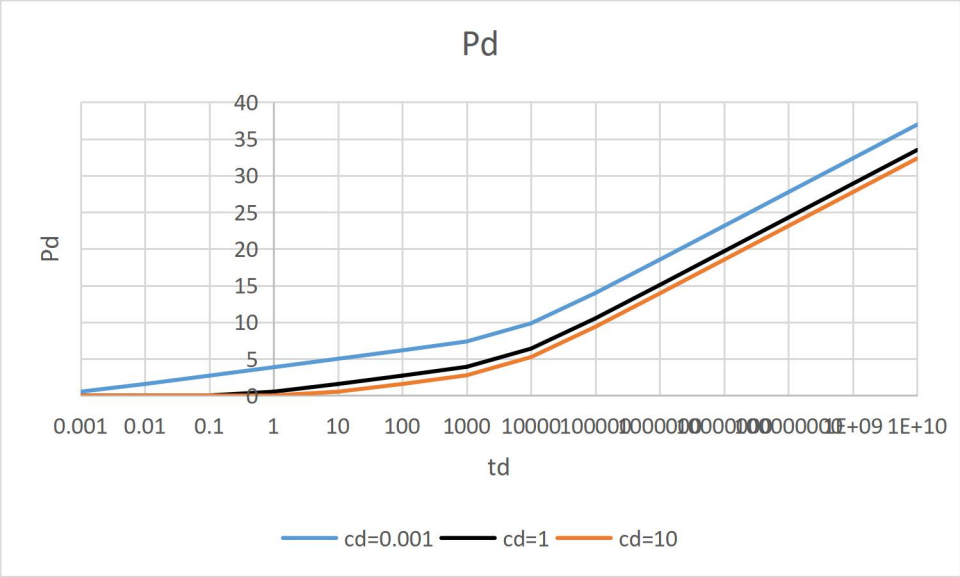

Figure 4.19 Graph of Dimensionless pressure against dimensionless time

- Table 4.57 Dimensionless pressure for skin 10 at different cd

t_D	cd= 0.001	cd=1	cd=10
	P_{DOW}	P_{DOW}	P_{DOW}
0.001	10.52214	10	10
0.01	11.56825	10	10
0.1	12.70837	10.01246	10
1	13.85854	10.52214	10.01246
10	15.00972	11.56825	10.52214
100	16.161	12.70837	11.56825
1000	17.36792	13.91417	12.764
10000	19.84039	16.38652	15.23534
100000	23.97271	20.51883	19.36755
1000000	28.5235	25.06962	23.91833
10000000	33.12315	29.66927	28.51798
1E+08	37.72776	34.27389	33.12259
1E+09	42.33288	38.879	37.72771
1E+10	46.93804	43.48417	42.33287

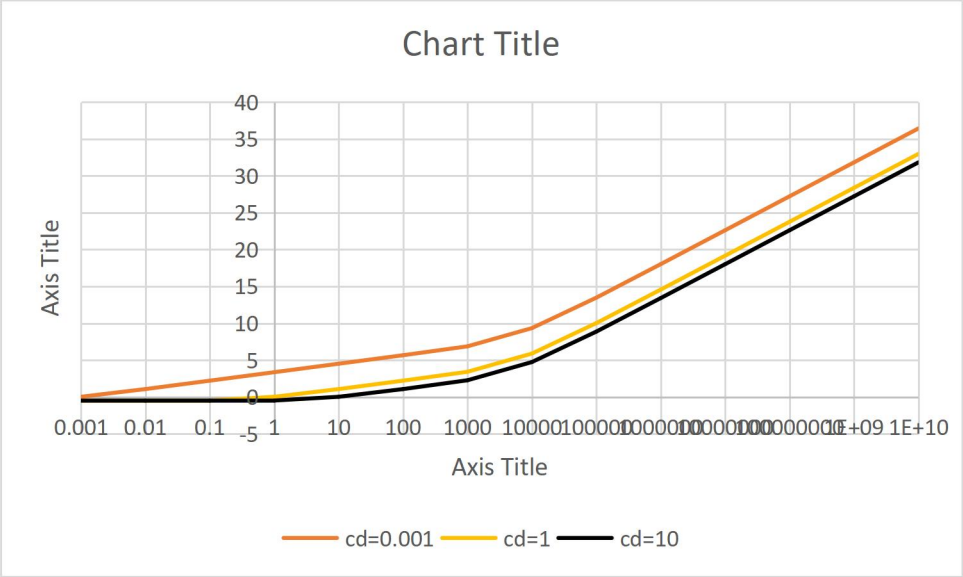

Figure 4.20 Graph of Dimensionless pressure against dimensionless time

❖ Graph of skin against P'_{DOW} for all the different cd

- Table 4.58 Dimensionless pressure derivative for skin -0.5 at different cd

t_D	cd=0.001	cd=1	cd =10
	P'_{DOW}	P'_{DOW}	P'_{DOW}
0.001	0.3894	0	0
0.01	0.487655	0	0
0.1	0.498752	0	0
1	0.499875	0.04	0.04
10	0.499988	0.39	0.39
100	0.499999	0.49	0.49
1000	0.642129	0.58	0.64
10000	1.535903	1.46	1.54
100000	1.9404	1.93	1.94
1000000	1.993874	1.99	1.99
10000000	1.999386	2	2
1E+08	1.999939	2	2
1E+09	1.999994	2	2
1E+10	1.999999	2	2

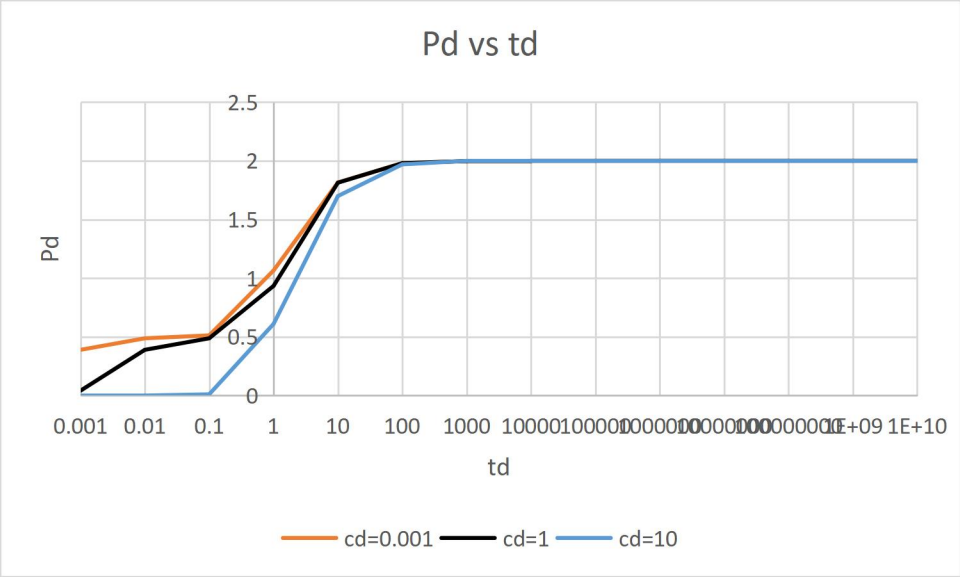

Figure 4.21Graph of Dimensionless pressure derivative against dimensionless time

- Table 4.59 Dimensionless pressure derivative for skin 0 at different cd

t_D	cd=0.001	cd=1	cd =10
	P'_{DOW}	P'_{DOW}	P'_{DOW}
0.001	0.3894	0	0
0.01	0.487655	0	0
0.1	0.498752	0	0
1	0.499875	0.04	0.04
10	0.499988	0.39	0.39
100	0.499999	0.49	0.49
1000	0.642129	0.58	0.64
10000	1.535903	1.46	1.54
100000	1.9404	1.93	1.94
1000000	1.993874	1.99	1.99
10000000	1.999386	2	2
1E+08	1.999939	2	2
1E+09	1.999994	2	2
1E+10	1.999999	2	2

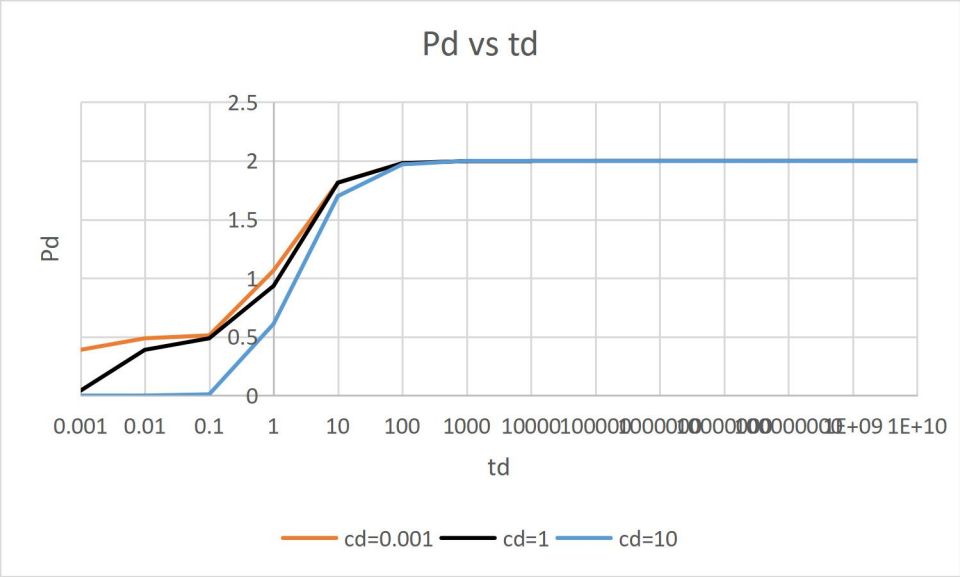

Figure 4.22Graph of Dimensionless pressure derivative against dimensionless time

- Table 4.60 Dimensionless pressure derivative for skin 10 at different cd

t_D	cd=0.001	cd=1	cd =10
	P'_{DOW}	P'_{DOW}	P'_{DOW}
0.001	0.3894	0	0
0.01	0.487655	0	0
0.1	0.498752	0	0
1	0.499875	0.04	0.04
10	0.499988	0.39	0.39
100	0.499999	0.49	0.49
1000	0.642129	0.58	0.64
10000	1.535903	1.46	1.54
100000	1.9404	1.93	1.94
1000000	1.993874	1.99	1.99
10000000	1.999386	2	2
1E+08	1.999939	2	2
1E+09	1.999994	2	2
1E+10	1.999999	2	2

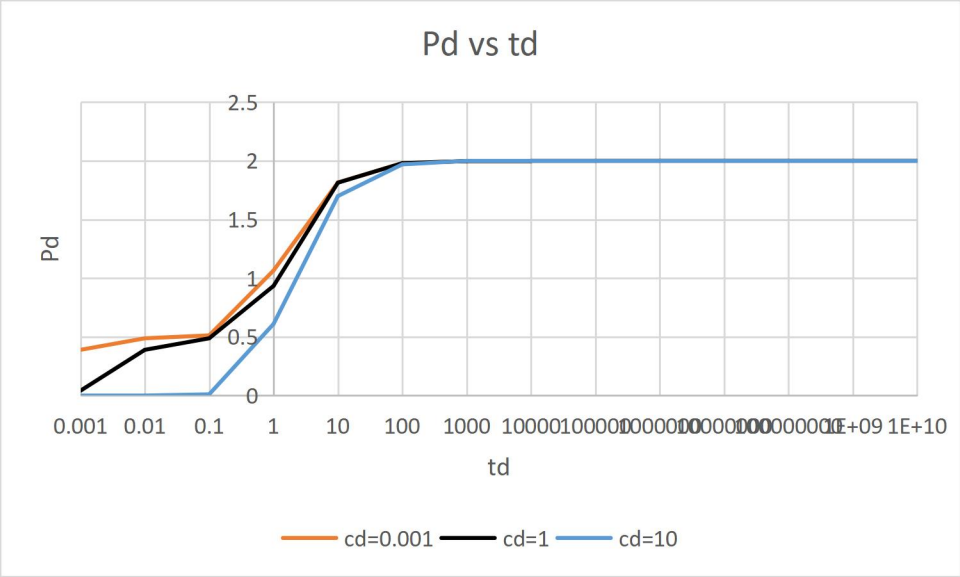

Figure 4.23Graph of Dimensionless pressure derivatives against dimensionless time

4.2 DISCUSSION OF RESULT

4.2.1 For comparing close and equal distance to the faults for d_1 and d_3

The different distances from the boundary can affect the drainage area and the efficiency of reservoir depletion. The well is too close to the boundary, it might lead to early water or gas breakthrough.

4.2.1.1 Zero skin

Zero skin indicates no resistance to flow near the wellbore, which suggests an efficient well completion and good reservoir connectivity. This means the well would be able to produce at optimal rates without any hindrance from near wellbore conditions. Considering the different wellbore storage;

- For the wellbore storage cd=10 shows that the well has a significant capacity to store fluids within the wellbore. This can lead to high initial production rates as the stored fluids are produced, but these rates may not be sustainable as they do not necessarily reflect the long-term production capacity of the reservoir. The zero skin value is favorable, but the high wellbore storage and varying distance from the boundary require careful reservoir management to optimize production and extend the life of the well.

- For Wellbore storage cd=1 shows that the well has a moderate capacity to store fluids within the wellbore. This can lead to a buffering effect where the wellbore fluid contributes to production before the reservoir fluid significantly impacts the flow rate. However, this can also affect the pressure transient behavior during

well testing, as the wellbore storage can mask the true reservoir characteristics until the stored fluids have been produced

- For Wellbore storage cd=0.001, It suggests that the well will have a rapid pressure response to changes in production rates, which can be beneficial for early detection of reservoir behavior but may also require careful management to avoid rapid depletion

4.2.1.2 Positive skin

This indicates that there may be some form of restriction or additional resistance to flow near the wellbore. This could be due to formation damage, poor completion practices, or other factors that impede the flow of fluids into the wellbore. A positive skin value generally leads to a decrease in production efficiency because it requires a higher pressure differential to achieve the same flow rate as a well with a zero or negative skin value

- For Wellbore storage cd=10 , suggests that the well has a significant capacity to store fluids within the wellbore. In terms of production, this means that there is a buffer of fluid available that can initially contribute to production rates

- For Wellbore storage cd=1, it suggests that the well has a moderate capacity to store fluids within the wellbore. This can lead to a buffering effect where the wellbore fluid contributes to production before the reservoir fluid significantly impacts the flow rate. However, this can also affect the pressure transient behavior during well testing, as the wellbore storage can mask the true reservoir characteristics until the stored fluids have been produced

- For wellbore storage cd=0.001,It indicate that the well will have a rapid pressure response to changes in production rates, this is beneficial for early detection of reservoir behavior but may also require careful management to avoid rapid depletion

4.2.1.3 Negative skin

This indicates that there may be some form of restriction or additional resistance to flow near the wellbore. This could be due to formation damage, poor completion practices, or other factors that impede the flow of fluids into the wellbore. A positive skin value generally leads to a decrease in production efficiency because it requires a higher pressure differential to achieve the same flow rate as a well with a zero or negative skin value

- For wellbore storage cd=10 it indicates plies a large capacity for fluid storage in the wellbore, which can result in high initial production rates. However, these

rates may not be sustainable as they might not reflect the reservoir's long-term production capacity.

- For wellbore storage cd=1 it suggests that the well has a moderate capacity to store fluids within the wellbore. This can lead to a buffering effect where the wellbore fluid contributes to production before the reservoir fluid significantly impacts the flow rate. However, this can also affect the pressure transient behavior during well testing, as the wellbore storage can mask the true reservoir characteristics until the stored fluids have been produced
- For wellbore storage cd=0.001, It can lead to a rapid pressure response to changes in production rates, which can be beneficial for early detection of reservoir behavior but may also require careful management to avoid rapid depletion

4.2.1 For comparing close and different distance to the faults for d_1 and d_3

The different distances from the boundary can affect the drainage area and the efficiency of reservoir depletion. The well is too close to the boundary; it might lead to early water or gas breakthrough.

4.2.1.1 Zero skin

Zero skin indicates no resistance to flow near the wellbore, which suggests an efficient well completion and good reservoir connectivity. This means the well would be able to produce at optimal rates without any hindrance from near wellbore conditions. Considering the different wellbore storage;

- For the wellbore storage cd=10 shows It means that during production, a considerable amount of fluid can be produced initially from the wellbore storage itself before the reservoir fluid starts contributing significantly to the production.

- For Wellbore storage cd=1 indicating a significant volume of fluid can be stored in the wellbore, this can have a substantial impact on the well's pressure behavior, especially during transient testing. It can lead to a larger initial pressure drop and a longer period before the well reaches pseudo-steady state production

- For Wellbore storage cd=0.001 It suggests that the well has a small capacity to store fluids, which can lead to rapid pressure changes in response to production rates

4.2.2 Positive skin

This indicates that there may be some form of restriction or additional resistance to flow near the wellbore. This could be due to formation damage, poor completion practices, or other factors that impede the flow of fluids into the wellbore. A positive skin value generally leads to a decrease in production efficiency because it requires a higher pressure differential to achieve the same flow rate as a well with a zero or negative skin value

- For wellbore storage cd=10The positive skin value is not ideal, but the high wellbore storage and varying distance from the boundary require careful reservoir management to optimize production and extend the life of the well.
- For wellbore storage cd=1, it suggests that the well has a moderate capacity to store fluids within the wellbore. This can lead to a buffering effect where the wellbore fluid contributes to production before the reservoir fluid significantly impacts the flow rate. However, this can also affect the pressure transient behavior during well testing, as the wellbore storage can mask the true reservoir characteristics until the stored fluids have been produced
- For wellbore storage cd=0.001 It suggests that the well will have a rapid pressure response to changes in production rates, which can be beneficial for early detection of reservoir behavior but may also require careful management to avoid rapid depletion

4.2.3 Negative skin

This indicates that there may be some form of restriction or additional resistance to flow near the wellbore. This could be due to formation damage, poor completion practices, or other factors that impede the flow of fluids into the wellbore. A positive skin value generally leads to a decrease in production efficiency because it requires a higher pressure differential to achieve the same flow rate as a well with a zero or negative skin value

- For wellbore storage cd=10 it indicates value is the suggesting that the well has a significant capacity to store fluids. In practical terms, this means that a large volume of fluid can be produced from wellbore storage alone, especially at the beginning of production. This can lead to high initial production rates, but these rates may not be sustainable as they do not necessarily reflect the long-term production capacity of the reservoir.

- For wellbore storage cd=1 it indicates a moderate amount of fluid storage within the wellbore. During production, this can lead to a buffering effect where the wellbore fluid contributes to production before the reservoir fluid significantly impacts the flow rate

- For wellbore storage cd=0.001,It suggests that the well will have a rapid pressure response to changes in production rates, which can be beneficial for early detection of reservoir behavior but may also require careful management to avoid rapid depletion.

CHAPTER FIVE

5 CONCLUSION AND RECOMMENDATION

5.1 CONCLUSION

In conclusion, the study on Dimensionless Pressure and Pressure Derivative Responses of a Vertical Well Completed in a Reservoir with Impermeable Boundaries Inclined at Right Angle has provided valuable insights into the dynamic behavior of such wells. From the results obtained, several key conclusions can be drawn:

1. Boundary Effects: Strategic Well Placement: Wells positioned farther from impermeable boundaries experience less perturbation due to their sealing effect. This highlights the importance of thoughtful well placement to mitigate reservoir disturbances.
2. Boundary Geometry: Variations in dimensionless pressure responses according to different boundary angles underscore the complex interplay between boundary geometry and reservoir behavior. Comprehensive reservoir characterization is essential to understand these effects.
3. Long-Term Production Trend: The observation of a constant pressure gradient at late dimensionless time indicates a predictable long-term production trend. This insight offers valuable forecasting information for reservoir management.
4. Reservoir Performance Implications: These findings have significant implications for both short-term and long-term reservoir performance. Accurate analysis and strategic decision-making are crucial in reservoir engineering. Understanding the impact of impermeable boundaries and wellbore storage on pressure behavior allows engineers to optimize production and enhance recovery.

In summary, this study contributes to our understanding of well behavior near boundaries and provides actionable insights for reservoir management.

5.2 RECOMMENDATION

"Moving forward, several recommendations emerge from the study on Dimensionless Pressure and Pressure Derivative Responses of a Vertical Well Completed in a Reservoir with Impermeable Boundaries Inclined at Right Angle:

1. Explore Boundary Angles: Conduct further research exploring angles beyond the commonly studied ones (e.g., 23°, 56°, 17°, etc.). A more comprehensive understanding of boundary effects on dimensionless pressure behavior can be gained by examining a wider range of boundary angles.
2. Consider Reservoir Thickness and Well Length: Investigate the influence of reservoir thickness and well length on dimensionless pressure responses. These factors significantly impact reservoir performance and production optimization strategies. Understanding their effects can lead to more informed decisions in reservoir engineering.
3. Optimize Well Placement: To enhance production efficiency, prioritize drilling wells at considerable distances from impermeable boundaries. The study observed that wells positioned farther from boundaries experienced reduced perturbations due to boundary sealing effects. Strategic well placement is essential for maximizing field productivity.
4. Strategic Decision-Making: Implement well placement practices that consider reservoir geometry, boundary conditions, and well interaction dynamics. Strategic decisions based on these factors can lead to improved reservoir performance and long-term production sustainability."

REFERENCES

Abbaszadeh, M., Evaluation, P. H.-S. F., & 1990, undefined. (n.d.). Pressure-transient analysis for a slanted well in a reservoir with vertical pressure support. *Onepetro.Org*. Retrieved April 12, 2024, from https://onepetro.org/FE/article/5/03/277/168477

E.S, A., & O., B. K. (n.d.). *Application of Gauss- Laguerre Quadrature in Computing Exponential Integral Function, Ei*.

Edobhiye, O., & Adewole, E. S. (2014). Effects of Both Wellbore and Reservoir Properties on Dimensionless Pressure and Dimensionless Pressure Derivative Distribution of a Horizontal Well in a Reservoir Subject to Bottom Water, Gas Cap and Single Edge Water Drive Mechanisms. *38th Nigeria Annual International Conference and Exhibition, NAICE 2014 - Africa's Energy Corridor: Opportunities for Oil and Gas Value Maximization Through Integration and Global Approach*, *1*, 439–450. https://doi.org/10.2118/172384-MS

Escobar, F. H., Suescún-Díaz, D., & Galindo, J. M. (2020). *PRESSURE AND PRESSURE DERIVATIVE ANALYSIS WITH INTER-RESERVOIR CROSS FLOW RATE BETWEEN ADJACENT RESERVOIR LAYERS*. *15*(22). www.arpnjournals.com

Eziuzor, D., Conference, S. A.-S. N. A. I., & 2022, undefined. (n.d.). Type Curves of a Vertical Well Completed Within a Pair of Inclined Sealing Faults. *Onepetro.Org*. Retrieved April 12, 2024, from https://onepetro.org/SPENAIC/proceedings-abstract/22NAIC/3-22NAIC/495008

Ganat, T. A.-A. O. (2023). *The Principle of Superposition*. 137–151. https://doi.org/10.1007/978-3-031-28889-0_6

H., C.-L., F., S.-V., & N., D.-A. (n.d.). Transient Pressure Behavior for a Well With a Finite-Conductivity Vertical Fracture. *SPEJ*, 253–264.

Jr, H. R., Journal, R. A.-S. of P. E., & 1972, undefined. (n.d.). Annulus unloading rates as influenced by wellbore storage and skin effect. *Onepetro.Org*. Retrieved April 12, 2024, from https://onepetro.org/spejournal/article-abstract/12/05/453/163971

Kartoatmodjo, R. S. T. (2016). *Type Curve Analysis*. 112–183.

Khan, S., Khulief, Y. A., & Al-Shuhail, A. A. (2020). Effects of reservoir size and boundary conditions on pore-pressure buildup and fault reactivation during CO2 injection in deep geological reservoirs. *Environmental Earth Sciences*, *79*(12), 1–23. https://doi.org/10.1007/S12665-020-09040-0/METRICS

Kuchuk, F. J., Goode, P. A., Wilkinson, D. J., & Thambynayagam, R. K. M. (1991).

Pressure-Transient Behavior of Horizontal Wells With and Without Gas Cap or Aquifer. *SPE Formation Evaluation*, *6*(01), 86–94. https://doi.org/10.2118/17413-PA

Lu, J., Yang, E., Rahman, M. M., & Wang, X. (2023). Effects of Reservoir Boundary Conditions, Drainage Shape, and Well Location on Productivity of a Vertical Well. *Journal of GeoEnergy*, *2023*, 1–14. https://doi.org/10.1155/2023/5745180

Matthews, C. S. (1986). Transient, Semisteady-State, and Steady-State Flow. *Journal of Petroleum Technology*, *38*(04), 385–386. https://doi.org/10.2118/15278-PA

Ogbamikhumi, A., International, E. A.-S. N. A., & 2021, undefined. (n.d.). Characteristics of dimensionless pressure gradients and derivatives of horizontal and vertical wells completed within inclined sealing faults. *Onepetro.Org*. Retrieved April 12, 2024, from https://onepetro.org/SPENAIC/proceedings-abstract/21NAIC/3-21NAIC/465667

Ojukwu, I. N., Adewole, E. S., & Taiwo, O. A. (2023). Dimensionless Pressures and Their Derivatives for a Vertical WellCompleted within a Pair of Inclined Constant-Pressure Boundaries. *Society of Petroleum Engineers - SPE Nigeria Annual International Conference and Exhibition, NAIC 2023*. https://doi.org/10.2118/217112-MS

Olaya-Marin, G., Escobar, F. H., & Robayo, F. (2020). *PRESSURE AND PRESSURE DERIVATIVE INTERPRETATION FOR VERTICAL WELLS IN NATURALLY FRACTURED AND COMPRESSIBLE FORMATIONS*. *15*(7). www.arpnjournals.com